Urology Research

Editors-in-Chief

Arnold P. P. Achermann

University of Campinas, Brazil

Yunshan Zhang

Affiliated Hospital of Guangdong Medical University, China

BIO-BYWORD SCIENTIFIC PUBLISHING PTY LTD
(619 649 400)
Level 10
50 Clarence Street
SYDNEY NSW 2000
Copyright © 2026. Bio-Byword Scientific Publishing Pty Ltd.
Complimentary Copy



Urology Research

Focus and Scope

Urology Research publishes peer-reviewed research articles across basic, translational, and clinical Urology medicine. The Journal covers all aspects of Urology medicine (full listing below) with an emphasis on studies that challenge the status quo of treatments and practices in Urology care or facilitate the translation of scientific advances into the clinic as new therapies or diagnostic tools.

About Publisher

Bio-Byword Scientific Publishing is a fast-growing, peer-reviewed and open access journal publisher, which is located in Sydney, Australia. As a dependable and credible corporation, it promotes and serves a broad range of subject areas for the benefit of humanity. By informing and educating a global community of scholars, practitioners, researchers and students, it endeavors to be the world's leading independent academic and professional publisher. To realize it, it keeps creative and innovative to meet the range of the authors' needs and publish the best of their work.

By cooperating with University of Sydney, University of New South Wales and other world-famous universities, Bio-Byword Scientific Publishing has established a huge publishing system based on hundreds of academic programs, and with a variety of journals in the subjects of medicine, construction, education and electronics.

Publisher Headquarter

BIO-BYWORD SCIENTIFIC PUBLISHING PTY LTD
Level 10
50 Clarence Street
Sydney NSW 2000
Website: www.bbwpublisher.com
Email: info@bbwpublisher.com

2026, Volume 4, Issue 3

Table of Contents

1 **Analysis of the Short-Term Efficacy and Safety of Single-Plane Retroperitoneal Laparoscopic Adrenalectomy for Adrenal Adenomas ≤ 5 cm**
Chaohua Zhang, Lijun Shao, Kaixiong Zhang

8 **Combined Use of PI-RADS, PSA Density, and the Free-to-Total PSA Ratio for Prostate Cancer Diagnosis in the PSA Gray Zone: A Narrative Review**
Tao Liu

15 **Identification of Key Targets for Proton Pump Inhibitors Induced Tubulointerstitial Nephritis Based on Pharmacovigilance and Network Toxicology Analysis**
Haolong Li, Zhu Wang, Hui Liang

30 **Application of Distal Urethral Mobilization in the Duckett Procedure for Hypospadias**
Yi Wang, Shuai Han, Linlin Fan, Liwei Li

Urology Research, 2026, Volume 4, Issue 3
https://bbwpublisher.com/journal/UR
Online ISSN: 2981-8230
Print ISSN: 3083-4910

Analysis of the Short-Term Efficacy and Safety of Single-Plane Retroperitoneal Laparoscopic Adrenalectomy for Adrenal Adenomas ≤ 5 cm

Chaohua Zhang, Lijun Shao, Kaixiong Zhang

Baoding No.1 Hospital, Baoding 071000, Hebei, China

Copyright: © 2026 Author(s). This is an open-access article distributed under the terms of the Creative Commons Attribution License (CC BY 4.0), permitting distribution and reproduction in any medium, provided the original work is cited.

Abstract: *Objective*: To investigate the short-term clinical efficacy and surgical safety of single-plane retroperitoneal laparoscopic adrenalectomy for adrenal adenomas with a diameter ≤ 5 cm, and to provide an objective basis for the selection of clinical minimally invasive surgical procedures. *Methods*: A total of 50 patients with unilateral adrenal adenomas (all with tumor diameters ≤ 5 cm) who were admitted to our hospital between December 2020 and December 2025 were selected as study subjects. They were randomly assigned to an observation group (25 cases) and a control group (25 cases) using a random number table. The observation group underwent single-plane retroperitoneal laparoscopic adrenalectomy, while the control group underwent traditional multi-plane retroperitoneal laparoscopic adrenalectomy. Surgical-related indicators (operative time, intraoperative blood loss, and intraoperative conversion to open surgery rate), postoperative recovery indicators (postoperative drainage tube indwelling time, time to ambulation after surgery, postoperative hospital stay, and postoperative pain score), the incidence of postoperative complications, and changes in adrenal-related biochemical indicators before and after surgery were compared between the two groups. *Results*: All surgeries were successfully completed without any cases requiring conversion to open surgery during the operation. The operative time and intraoperative blood loss in the observation group were significantly better than those in the control group ($p < 0.05$). The postoperative drainage tube indwelling time, time to ambulation, and hospital stay in the observation group were significantly shorter than those in the control group, and the 24-hour postoperative Visual Analog Scale (VAS) pain score was significantly lower in the observation group (all $p < 0.001$). The incidence of complications in the observation group was lower than that in the control group, but the difference was not statistically significant ($\chi^2 = 2.000$, $p = 0.157 > 0.05$). One week after surgery, the aforementioned indicators in both groups had significantly improved compared with their pre-surgery values ($p < 0.05$). There was no significant difference in the biochemical indicators between the two groups one week after surgery ($p > 0.05$). *Conclusion*: Single-plane retroperitoneal laparoscopic adrenalectomy for adrenal adenomas ≤ 5 cm in diameter can significantly shorten operative time, reduce intraoperative blood loss, accelerate postoperative recovery, and lower the risk of postoperative complications. It has definite short-term efficacy and high safety, and the operation is simpler, making it suitable for clinical promotion and application.

Keywords: Single-plane retroperitoneal laparoscopy; Adrenalectomy; Adrenal adenoma; Short-term efficacy; Safety

Online publication: October 20, 2026

1. Introduction

Adrenal adenoma is a common benign tumor located in the adrenal gland in clinical practice, and its incidence has been increasing year by year. Most patients are accompanied by primary aldosteronism, hypercortisolism, or non-functional adenomas. Benign adenomas with a tumor diameter ≤ 5 cm are the core indications for minimally invasive treatment in urology [1]. Traditional open surgery has disadvantages such as significant trauma, slow postoperative recovery, and a high incidence of complications, so it has gradually been replaced by laparoscopic surgery. Retroperitoneal laparoscopic adrenalectomy can avoid interference with intra-abdominal organs, has a minor impact on the gastrointestinal tract, and enables rapid postoperative recovery, making it an ideal choice for the treatment of adrenal adenomas [2,3]. Traditional retroperitoneal laparoscopic adrenalectomy mostly adopts a multi-plane separation method, which requires sequential separation of multiple anatomical layers around the adrenal gland. The operative steps are cumbersome and require a high level of operator proficiency in anatomy, resulting in a relatively long operative time. Moreover, it is prone to damaging surrounding blood vessels, the peritoneum, and renal tissues during the operation, increasing the risk of intraoperative bleeding and postoperative complications. Single-plane retroperitoneal laparoscopic adrenalectomy is an improved minimally invasive surgical procedure. It achieves precise separation through a single anatomical plane, simplifies the surgical process, and reduces the scope of tissue dissection. Theoretically, it can further improve surgical efficiency and safety [4]. At present, there are still relatively few large-sample controlled studies on this surgical procedure for the treatment of adrenal adenomas ≤ 5 cm in diameter in clinical practice. This study selected 50 patients who met the inclusion criteria and conducted a group-controlled analysis to systematically evaluate their short-term efficacy and safety, providing data to support the optimization of clinical surgical procedures. The report is as follows.

2. Materials and methods

2.1. General information

Fifty patients with unilateral adrenal adenoma who were admitted to the urology department of our hospital from January 2022 to January 2025 were selected as study subjects.

2.1.1. Inclusion criteria

(1) Diagnosed as unilateral adrenal adenoma by abdominal CT, MRI, and endocrine examination, with a maximum tumor diameter ≤ 5 cm;
(2) Met surgical indications without contraindications;
(3) Aged 18–75 years, with ASA classification grades I-II;
(4) Complete clinical data, voluntary participation in this study, and signed informed consent.

2.1.2. Exclusion criteria

(1) Malignant adrenal tumors or metastatic tumors;
(2) Tumor diameter > 5 cm;
(3) Combined with severe cardiac, hepatic, renal, or coagulation dysfunction;
(4) Previous history of retroperitoneal surgery or severe abdominal adhesions;
(5) Functional adenoma with uncontrolled severe endocrine disorders;
(6) Pregnant or lactating women.

2.1.3. Study design

The 50 patients were randomly divided into an observation group and a control group using a random number table method, with 25 cases in each group.

(1) Observation group

11 males and 14 females; aged 32–68 years, with an average age of 46.52 ± 8.36 years; tumor diameter ranging from 1.20 to 4.85 cm, with an average of 3.12 ± 0.85 cm; 13 cases of non-functional adenoma, 8 cases of primary aldosteronoma, and 4 cases of cortisol adenoma; 14 cases of left-sided lesions and 11 cases of right-sided lesions.

(2) Control group

12 males and 13 females; aged 30–70 years, with an average age of 45.89 ± 9.12 years; tumor diameter ranging from 1.15 to 4.90 cm, with an average of 3.08 ± 0.92 cm; 12 cases of non-functional adenoma, 9 cases of primary aldosteronoma, and 4 cases of cortisol adenoma; 13 cases of left-sided lesions and 12 cases of right-sided lesions. There were no statistically significant differences in baseline characteristics, including gender, age, tumor diameter, adenoma type, and affected side, between the two groups ($p > 0.05$), indicating clinical comparability.

2.2. Surgical methods

Both groups of patients underwent surgery performed by the same team of experienced urologists under general anesthesia with tracheal intubation, lying on the healthy side with the waist bridge elevated, and routine disinfection and draping.

The control group underwent traditional multi-plane retroperitoneal laparoscopic adrenalectomy. The method of establishing the retroperitoneal space and the positions of the operative ports were the same as those in the observation group. After establishing pneumoperitoneum, the renal fascia, upper pole, lateral side, lower pole, and medial side of the adrenal gland were sequentially separated at multiple anatomical levels to progressively free the entire adrenal gland. After fully exposing the adenoma, the central vein was ligated and cut, and the adenoma was completely resected. During the operation, the surrounding adhesive tissue was stripped layer by layer, a drainage tube was placed after hemostasis was achieved, and the incision was closed.

The observation group underwent single-plane retroperitoneal laparoscopic adrenalectomy. A 2 cm oblique incision was made at the lower edge of the 12th rib along the posterior axillary line. The skin, subcutaneous tissue, and lumbar dorsal fascia were successively incised, and the retroperitoneal space was bluntly separated with fingers. A balloon dilator was placed, and 300 mL of air was injected to expand the retroperitoneal space, thereby establishing an operative space. A laparoscope was placed, and the pneumoperitoneum pressure was maintained at 12-14 mmHg. Operative ports of 5 mm and 10 mm were made below the costal arch along the anterior axillary line and above the iliac crest along the mid-axillary line, respectively, serving as auxiliary operative channels. The anatomical landmarks of the renal fascia, psoas major muscle, and upper pole of the kidney were identified. Precise separation was performed along the single avascular plane between the dorsal side of the kidney and the adrenal gland, avoiding surrounding blood vessels and vital tissues, thereby directly exposing the adrenal adenoma and the adrenal gland's central vein. The central vein was first ligated and cut, and then the adenoma was completely stripped, avoiding extensive stripping of the surrounding adrenal tissue. Strict hemostasis was performed during the operation. After the operation, the wound was checked for active bleeding, one retroperitoneal drainage tube was placed, and the incision was closed layer by layer.

2.3. Observation indicators

(1) Surgical-related indicators

The operative time, intraoperative blood loss, and intraoperative conversion rate to open surgery were recorded for both groups. The operative time was calculated from the skin incision to the completion of the incision suture. The intraoperative blood loss was calculated using the aspirator measurement and gauze-weighing method.

(2) Postoperative recovery indicators

The duration of retroperitoneal drainage tube placement, time to first ambulation after surgery, and postoperative hospital stay were recorded. The visual analog scale (VAS) was used to assess the pain level 24 hours after surgery, with scores ranging from 0 to 10. Higher scores indicated more severe pain.

(3) Incidence of postoperative complications

The occurrences of postoperative complications such as subcutaneous emphysema, peritoneal injury, incision infection, perirenal hematoma, and worsening of endocrine disorders were counted, and the overall incidence was calculated.

(4) Biochemical indicators

Serum cortisol, aldosterone, and renin levels were measured before surgery and 1 week after surgery in both groups to evaluate the effect of surgery on endocrine function.

2.4. Statistical methods

Data analysis was performed using SPSS version 26.0. Measurement data were expressed as (± s), and comparisons between groups were made using independent sample *t*-tests, while comparisons within groups were made using paired sample *t*-tests. Count data were expressed as [n (%)], and comparisons between groups were made using χ^2 tests. A p-value < 0.05 was considered statistically significant.

3. Results

3.1. Comparison of surgical-related indicators between the two groups

All surgeries were successfully completed without any cases of intraoperative conversion to open surgery. The operative time and intraoperative blood loss in the observation group were significantly better than those in the control group ($p < 0.05$). See **Table 1** for details.

Table 1. Comparison of surgical-related indicators between the two groups

Group	Operation time (min)	Intraoperative blood loss (mL)	Conversion to open surgery rate [n (%)]
Observation group (n = 25)	30.00 ± 2.45	18.25 ± 4.36	0 (0.00)
Control group (n = 25)	45.68 ± 5.32	36.72 ± 7.89	0 (0.00)
t/χ^2	13.430	10.243	-
p	< 0.001	< 0.001	

3.2. Comparison of postoperative recovery indicators between the two groups

The observation group had significantly shorter postoperative drainage tube indwelling time, time to ambulation, and hospital stay compared with the control group. Additionally, the VAS pain score at 24 hours postoperatively was significantly lower in the observation group than in the control group (all $p < 0.001$). See

Table 2 for details.

Table 2. Comparison of postoperative recovery indicators between the two groups

Group	Drainage tube indwelling time (d)	Ambulation time (h)	Length of hospital stay (d)	Postoperative 24 h VAS score (points)
Observation group (n = 25)	1.20 ± 0.35	18.40 ± 3.26	3.15 ± 0.68	2.15 ± 0.58
Control group (n = 25)	2.35 ± 0.52	32.60 ± 5.48	5.20 ± 0.95	4.32 ± 0.76
t	9.177	11.146	8.725	11.321
p	< 0.001	< 0.001	< 0.001	< 0.001

3.3. Comparison of postoperative complication rates between the two groups

In the observation group, only one case of mild subcutaneous emphysema occurred postoperatively, which resolved spontaneously without special treatment, resulting in a total complication rate of 4.00%. In the control group, there were two cases of subcutaneous emphysema, one case of peritoneal injury, and one case of incision infection postoperatively, all of which healed after symptomatic treatment, leading to a total complication rate of 16.00%. The complication rate in the observation group was lower than that in the control group, but the difference was not statistically significant ($\chi^2 = 2.000$, $p = 0.157 > 0.05$). Neither group experienced severe complications such as perirenal hematoma, major vascular injury, or severe endocrine disorders, indicating good overall surgical safety.

3.4. Comparison of preoperative and postoperative biochemical indicators between the two groups

One week postoperatively, the aforementioned indicators in both groups showed significant improvement compared to preoperative values ($p < 0.05$). When comparing the biochemical indicators one week postoperatively between the two groups, no statistically significant difference was observed ($p > 0.05$). See **Table 3** for details.

Table 3. Comparison of preoperative and postoperative biochemical indicators between the two groups

Group	Time point	Cortisol (nmol/L)	Aldosterone (pmol/L)	Renin (μIU/L)
Observation group (n = 25)	Preoperative	456.32 ± 52.68	689.25 ± 75.36	125.68 ± 18.45
	1 week postoperative	325.46 ± 41.25	356.82 ± 42.36	78.35 ± 10.26
Control group (n = 25)	Preoperative	452.89 ± 50.36	685.46 ± 72.68	123.52 ± 17.92
	1 week postoperative	322.68 ± 43.59	352.96 ± 45.12	76.89 ± 11.35

4. Discussion

Adrenal adenoma is a common benign tumor in urological surgery, with minimally invasive surgery being the primary treatment approach. Retroperitoneal laparoscopic surgery has gradually replaced traditional open surgery due to its advantages of minimal trauma, precise positioning, and rapid postoperative recovery [5]. Traditional retroperitoneal laparoscopic adrenalectomy employs a multi-layer dissection technique, requiring comprehensive dissection of the tissues surrounding the adrenal gland. Although it can completely remove the tumor, the procedure is cumbersome, traumatic, time-consuming, and prone to causing damage to surrounding tissues. Particularly for physicians in primary healthcare institutions, it presents a steep learning

curve and carries significant surgical risks.

Single-plane retroperitoneal laparoscopic adrenalectomy is a novel minimally invasive surgical approach optimized based on anatomical considerations. The results of this study indicate that the average surgical time for this procedure is only 30.00 ± 2.45 minutes, significantly shorter than that of traditional methods. Intraoperative blood loss is only 18.25 ± 4.36 mL, substantially reducing intraoperative trauma. The core advantage of this approach lies in its precise positioning of a single avascular anatomical plane, eliminating the need for sequential dissection of multiple tissue layers and directly exposing the surgical target area, thereby shortening the operative process. Simultaneously, it reduces the stripping and damage to normal tissues, lowering the risk of bleeding [6]. In this study, there were no cases of conversion to open surgery in either group, confirming the high feasibility of the single-plane approach for adrenal adenomas ≤ 5 cm in diameter, with lower operational difficulty and easier mastery.

Postoperative recovery is a key indicator for evaluating the short-term efficacy of minimally invasive surgical approaches. In this study, the observation group had significantly shorter durations of postoperative drainage tube placement, time to ambulation, and hospital stay compared with the control group, as well as lower postoperative pain scores. This clearly demonstrates that the single-plane approach causes less trauma, effectively alleviates postoperative pain, accelerates recovery of gastrointestinal function and limb mobility, and shortens hospital stay, aligning with the principles of enhanced recovery after surgery [7,8]. Additionally, the postoperative complication rate in the observation group was only 4.00%, significantly lower than the 16.00% in the control group. This is primarily because single-plane dissection reduces the risk of peritoneal injury, subcutaneous emphysema, and incision infection, significantly enhancing surgical safety, consistent with findings from relevant domestic studies [9].

In terms of treatment efficacy, both groups showed significant improvements in postoperative adrenal-related biochemical indicators, with no between-group differences. This indicates that the single-plane approach, while simplifying the procedure and reducing time, does not compromise adenoma removal or endocrine function, achieving therapeutic outcomes comparable to traditional methods while balancing efficacy, efficiency, and safety [10]. For benign adrenal adenomas with a diameter ≤ 5 cm, the single-plane retroperitoneal laparoscopic adrenalectomy has clear indications and prominent advantages, particularly suitable for young patients, those with weaker physical conditions, and primary hospitals. It effectively reduces surgical difficulty and enhances surgical safety.

This study has certain limitations: the sample size is relatively small (only 50 cases); the follow-up period is short, evaluating only short-term efficacy and safety without long-term follow-up to assess tumor recurrence and late complications; and it is a single-center study, potentially subject to selection bias. Subsequent research should increase the sample size, conduct multicenter, long-term follow-up studies to further validate the long-term efficacy of this approach, refine indications for different types and sizes of adrenal adenomas, and improve surgical operative norms.

5. Conclusion

In conclusion, single-plane retroperitoneal laparoscopic adrenalectomy for adrenal adenomas with a diameter ≤ 5 cm demonstrates definite short-term clinical efficacy, significantly shortening surgical time, reducing intraoperative blood loss, accelerating postoperative recovery, and lowering the postoperative complication

rate. It offers high surgical safety, is simple and easy to learn, does not affect tumor removal efficacy or endocrine function improvement, and is an ideal minimally invasive surgical approach for treating adrenal adenomas ≤ 5 cm in diameter, and is worthy of promotion and application in clinical hospitals at all levels.

Funding

Feasibility and Safety Study of the Extraperitoneal Three-Plane Approach for Adrenal Tumor Resection(Project Number: 2641ZF029).

Disclosure statement

The authors declare no conflict of interest.

References

[1] Xu A, Sun S, Liu P, et al., 2023, Value Analysis of MSCT and 3.0T MRI in the Differential Diagnosis of Adrenal Tumors. Chinese Journal of CT and MRI, 21(10): 130–132.

[2] Zhang Z, Xie T, Liu L, et al., 2022, Efficacy Analysis of Suprapubic-Assisted Single-Port Laparoscopic Surgery Versus Retroperitoneal Laparoscopic Surgery for Adrenal Cysts. Journal of Clinical Urology, 37(05): 369–372.

[3] Wan S, Di J, Xi M, et al., 2018, Application of Direct-Vision One-Step Establishment of the Observation Mirror Channel in Transabdominal Laparoscopic Adrenalectomy. Chinese Journal of Endourology (Electronic Edition), 12(03): 159–163.

[4] Ma Y, Wei Y, Zhu Q, 2026, Preliminary Application Effect of a Domestically Produced Single-Port Laparoscopic Surgical Robot in Partial Nephrectomy (With Surgical Video). Journal of Robotic Surgery (Chinese-English Edition), 7(01): 23–27.

[5] Liu J, Liu M, 2025, Research Progress in Robot-Assisted Partial Nephrectomy for Complex Renal Tumors. Modern Journal of Urology, 30(11): 960–966.

[6] Internet Hospital Branch of the Chinese Research Hospital Association, 2022, Chinese Guidelines for Minimally Invasive Treatment Technologies for Tumors. Oncology Progress, 20(18): 1838–1856.

[7] Lu P, Chen L, Huang Y, et al., 2025, Super Minimally Invasive Laparoscopic Surgery: Technological Innovation and Clinical Research Progress. Chinese Journal of General Surgery, 34(10): 2265–2271.

[8] Huang Y, Li H, Zeng B, et al., 2023, Research Progress on the Development Status and Nursing Strategies of Day-Case Laparoscopic Cholecystectomy. Modern Medicine and Health, 39(02): 309–312 + 319.

[9] Ling Q, Wu T, Yang H, 2023, Clinical Effect of Retroperitoneal Laparoscopic Single-Anatomical-Plane Adrenal Tumor Resection for Large Adrenal Tumors with a Diameter > 6 cm. Clinical Medicine and Engineering, 30(05): 605–606.

[10] Li J, Li Q, Liu J, et al., 2019, Clinical Comparison Between Modified Single-Layer and Traditional Three-Layer Retroperitoneal Laparoscopic Adrenal Mass Resection. Journal of Bengbu Medical College, 44(09): 1227–1229.

Publisher's note

Bio-Byword Scientific Publishing remains neutral with regard to jurisdictional claims in published maps and institutional affiliations.

Urology Research, 2026, Volume 4, Issue 3
https://bbwpublisher.com/journal/UR
Online ISSN: 2981-8230
Print ISSN: 3083-4910

Combined Use of PI-RADS, PSA Density, and the Free-to-Total PSA Ratio for Prostate Cancer Diagnosis in the PSA Gray Zone: A Narrative Review

Tao Liu

The First Affiliated Hospital of Yangtze University, Jingzhou 434000, Hubei, China

Copyright: © 2026 Author(s). This is an open-access article distributed under the terms of the Creative Commons Attribution License (CC BY 4.0), permitting distribution and reproduction in any medium, provided the original work is cited.

Abstract: When total prostate-specific antigen (tPSA) is between 4 and 10 ng/mL, the result alone often cannot distinguish prostate cancer from benign prostatic disease. The combination of the Prostate Imaging Reporting and Data System (PI-RADS) score and PSA density (PSAD) provide additional information for biopsy decisions in this population. The free-to-total PSA ratio (f/tPSA) is another commonly used adjunct, although some evidence supporting its diagnostic value predates the widespread use of magnetic resonance imaging (MRI). This narrative review examines studies of these three measures, with particular attention to age, model composition, and biopsy outcomes. Available evidence supports combining PI-RADS with PSAD to improve risk stratification. The f/tPSA ratio has also shown diagnostic value in certain age groups and MRI-defined populations. However, good performance of a multivariable model does not establish that every included predictor provides additional information. In men aged ≥ 60 years with tPSA levels of 4–10 ng/mL, direct comparisons of models with and without f/tPSA are needed. Reporting both the number of biopsies avoided and the number of clinically significant cancers missed would help clarify the clinical value of the three-variable approach.

Keywords: Prostate cancer; PSA gray zone; PI-RADS; PSA density; Free-to-total PSA ratio; Combined diagnostic assessment

Online publication: October 20, 2026

1. Introduction

An elevated total prostate-specific antigen (tPSA) level is a common reason for further investigation of suspected prostate cancer. PSA is organ-specific, but its cancer specificity is limited: benign prostatic hyperplasia and inflammation can also increase serum concentrations. At tPSA levels of 4–10 ng/mL, commonly described as the PSA gray zone, the distributions observed in benign and malignant disease overlap. Identifying which patients should undergo biopsy is therefore a central purpose of research on

adjunctive diagnostic measures [1].

The free-to-total PSA ratio (f/tPSA) has long been used to assess patients in this range, principally as a supplement to tPSA testing [2]. With the introduction of prebiopsy magnetic resonance imaging (MRI), risk assessment has expanded to include lesion characteristics and prostate volume. The Prostate Imaging Reporting and Data System (PI-RADS) score describes the degree of suspicion on MRI, while PSA density (PSAD) relates tPSA to gland volume. Clinicians consequently have more information available than serum PSA measurements alone.

This change in practice raises a specific question about f/tPSA: once PI-RADS and PSAD are known, does the ratio improve risk estimates sufficiently to change biopsy decisions? Its sensitivity or specificity in isolation cannot answer that question. Age-stratified studies provide a rationale for examining men aged ≥ 60 years with PSA levels in the gray zone. This review considers that evidence alongside studies of combined diagnostic approaches and discusses the issues that affect their interpretation.

2. Literature sources and scope

This narrative review draws on literature concerning the PSA gray zone, MRI scoring, PSAD, f/tPSA, and age-stratified diagnosis. Study details were checked using PubMed-indexed records, full-text articles available through PubMed Central, and journal and guideline websites. The literature search for the review topic extended through September 9, 2026. Search terms included “prostate cancer”, “PSA gray zone”, “PI-RADS”, “PSA density”, “free-to-total PSA”, “percent free PSA”, “age”, and “prediction model”.

The discussion focuses on original studies involving patients with tPSA levels of 4–10 ng/mL. Studies of broader populations were also considered where they helped explain the performance of combined approaches; their eligibility criteria were taken into account when assessing applicability. This review did not include an exhaustive systematic search, independent duplicate screening, or a new quantitative synthesis.

3. The contribution of PSAD after MRI assessment

PI-RADS v2.1 assigns scores from 1 to 5 to describe the likelihood that an MRI finding represents clinically significant prostate cancer (csPCa). Diffusion-weighted imaging is the dominant sequence for peripheral-zone assessment, whereas T2-weighted imaging is dominant in the transition zone [3]. Standardized scoring supports communication of imaging findings and helps guide subsequent biopsy sampling.

The PRECISION trial enrolled 500 biopsy-naïve men with suspected prostate cancer. Clinically significant cancer was detected in 38% of patients assigned to the MRI pathway and 26% assigned to standard systematic biopsy [4]. These findings support the use of MRI before biopsy. However, the trial was not restricted to patients in the PSA gray zone, so its detection rates should not be treated as expected rates for that subgroup.

MRI does not resolve every biopsy decision. A PI-RADS score of 3 indicates an equivocal finding, and a negative MRI still requires interpretation alongside other clinical information. PSAD offers an additional measure in these circumstances and is calculated as follows:

PSAD = tPSA (ng/mL) / prostate volume (cm^3).

Patients with the same tPSA concentration may have substantially different PSAD values because their prostate volumes differ. Volume therefore helps place an elevated PSA result in context. The performance of PSAD nevertheless depends on the selected cutoff. In a meta-analysis of 39 studies, Wang et al. reported pooled sensitivities of 0.87, 0.61, and 0.42, and corresponding specificities of 0.39, 0.69, and 0.82, at PSAD thresholds of 0.10, 0.15, and 0.20 ng/mL/cm^3 in patients with PI-RADS or Likert scores of 3 [5]. Raising the cutoff reduced false-positive results but left more clinically significant cancers below the threshold.

Evidence more directly relevant to the gray zone comes from Wen et al., who retrospectively studied 453 patients. In the validation subset obtained by random splitting, the area under the receiver operating characteristic curve (AUC) for predicting csPCa was 0.871 for PI-RADS combined with PSAD, compared with 0.829 for PI-RADS alone and 0.677 for PSAD alone [6]. The results support the complementary value of imaging and density measurements. Because the validation data came from the same study cohort, performance at other centers remained unestablished.

The meta-analysis by Haj-Mirzaian et al. examined the implications for biopsy decisions. Strategies that omitted biopsy in patients with PI-RADS scores ≤ 3 and PSAD below 0.10 or 0.15 ng/mL/cm^3 could avoid approximately 30% and 48% of unnecessary biopsies, respectively, while maintaining overall strategy sensitivities of approximately 97% and 95% [7]. These estimates describe the strategies evaluated in the included populations. They do not imply that all patients with negative MRI findings have equivalent risk. Individual risk factors and arrangements for subsequent monitoring remain relevant when applying such strategies [1].

4. Earlier evidence for f/tPSA and the influence of age

4.1. From an adjunct to PSA testing to reassessment in the MRI era

The f/tPSA ratio expresses free PSA as a proportion of total PSA and may be reported as a decimal or percentage. Catalona et al. studied men with tPSA levels of 4–10 ng/mL and a nonsuspicious digital rectal examination. A percent-free PSA cutoff of 25% detected approximately 95% of cancers while avoiding approximately 20% of unnecessary biopsies [2]. This study provided an early basis for using f/tPSA in the PSA gray zone.

Its clinical setting matters when interpreting the findings. The outcome was detection of any prostate cancer, and contemporary MRI-based stratification was not part of the assessment. The study established that f/tPSA could supplement tPSA testing; it did not test its contribution after PI-RADS and PSAD had already been considered. As the information available for diagnosis expands, the additional contribution of an individual measure may change. Earlier diagnostic performance therefore cannot, by itself, establish that a three-variable approach is superior to a model using PI-RADS and PSAD.

4.2. Age-related findings in Chinese populations

Studies in Chinese populations have not produced entirely consistent results. Huang et al. evaluated 558 men with PSA levels of 2.5–20 ng/mL. Although cancer prevalence increased as percent-free PSA decreased, its AUC was not superior to that of PSA. Analyses stratified by age and prostate volume also did not demonstrate a clear advantage [8]. An association with cancer was therefore present without evidence of better discrimination than the existing test.

In contrast, the multicenter study by Chen et al. restricted PSA to 4–10 ng/mL and included 2,310 men undergoing an initial biopsy. The authors found that f/tPSA provided additional diagnostic value in men aged ≥ 60 years, whereas the same benefit was not observed in those aged 40–59 years [9]. Differences in PSA ranges, age categories, and patient composition prevent the disagreement between these studies from being attributed to a single factor. The latter study more closely matches the population of interest for research in older men with gray-zone PSA levels, but its principal comparison was still against PSA testing.

Another age-stratified study selected percent-free PSA cutoffs to detect 90% of prostate cancers. The resulting thresholds were 24%, 27%, and 32% for men aged 60–69, 70–79, and ≥80 years, respectively [10]. These differences suggest that a fixed cutoff may not perform equally across age groups. However, the thresholds were derived for a particular detection target in a specific sample and should not be adopted directly as universal biopsy criteria after MRI.

Together, these findings justify examining age while leaving an unresolved question: how much of the contribution observed for f/tPSA in men aged ≥ 60 years remains after PI-RADS and PSAD are included? Addressing this requires comparisons using the same patients and diagnostic outcome. Potential overlap between cohorts should also be checked when studies originate from the same research consortium and cover similar recruitment periods.

5. What studies of combined approaches can establish

5.1. Overall model performance and the contribution of an individual predictor

The term “combined” covers several different approaches in this literature. Some studies use a set of cutoffs to define biopsy rules; others develop multivariable prediction models or compare complete diagnostic pathways. Although each uses multiple measures, they do not necessarily answer the same question.

Baruah et al. prospectively enrolled 104 men with PSA levels of 4–10 ng/mL and lower urinary tract symptoms. They assessed different rules combining PI-RADS with PSAD or percent-free PSA, some of which improved specificity [11]. Their definition of csPCa incorporated Gleason score and cancer core length, and systematic biopsy served as the reference. The findings therefore describe the performance of particular decision rules rather than the incremental performance of a three-variable regression model.

Zhang et al. developed a nomogram containing age, PSAD, f/tPSA, and PI-RADS. Its validation-cohort AUC was 0.891, and the study reported improvement in net reclassification improvement (NRI) [12]. These findings might appear to establish the value of using all three diagnostic measures. However, the key comparison involved adding PI-RADS to an existing clinical model. The observed improvement primarily evaluated the inclusion of imaging information. To determine whether f/tPSA itself was needed, the appropriate comparison would retain the other predictors and remove only f/tPSA.

Liang et al. developed separate transition-zone and peripheral-zone models for patients with PI-RADS 3 findings. The transition-zone model retained age, f/tPSA, and PSAD, while the peripheral-zone model retained age, PSA, and prostate volume [13]. The different predictor sets suggest that the role of f/tPSA may depend on patient and lesion characteristics. Selection into a final model offers a reason for further investigation, but it does not quantify the clinical benefit obtained by adding the predictor.

Ding et al. developed a model in 155 patients with PSA levels in the gray zone that included f/tPSA, PI-RADS, and an elastography measure [14]. Because additional imaging information was incorporated, the results apply to that particular combination. Ranking the AUCs of models from separate studies would

confound differences in patient composition, outcome definitions, and predictor sets.

5.2. Changes in cancer detection accompanying biopsy avoidance

Diagnostic pathway studies can show the relationship between biopsy use and cancer detection more directly than AUC alone. Jin et al. evaluated 1,018 patients, including 378 with csPCa. The MRI-plus-PSAD pathway could avoid 302 biopsies while detecting 364 clinically significant cancers. The pathway that also incorporated f/tPSA could avoid 403 biopsies while detecting 357 clinically significant cancers [15].

Calculated from the reported counts, the three-measure pathway avoided 101 additional biopsies but detected seven fewer clinically significant cancers than the two-measure pathway. Adding f/tPSA therefore changed patient allocation, with reduced biopsy use accompanied by a loss in detection. Both outcomes are necessary to interpret the result. Net benefit was broadly comparable across the MRI-based combinations evaluated, and the study population was not restricted to the conventional PSA gray zone. The findings consequently do not establish which pathway should be preferred in men aged ≥ 60 years with PSA levels of 4–10 ng/mL.

Neither “f/tPSA adds no value” nor “the three-measure combination is better” adequately describes the current evidence. The incremental value depends on the population, comparator, decision threshold, and acceptable degree of missed cancer detection.

6. Factors affecting interpretation of combined diagnostic performance

Differences between studies begin with the diagnostic outcome. Any prostate cancer and csPCa are not interchangeable endpoints. Even studies reporting csPCa may use different definitions: some apply an International Society of Urological Pathology (ISUP) Grade Group threshold of ≥ 2, whereas others incorporate tumor volume or cancer core length [7,11,13]. Systematic and targeted biopsy also differ in sampling, which can affect the reference diagnosis. These features should be checked before comparing diagnostic performance.

Measurement methods are another source of variation. PSAD depends on prostate volume estimation, f/tPSA is calculated from two serum measurements, and PI-RADS assessment is influenced by image quality and interpretation [1,3]. Data used for combined modeling should, where possible, correspond to the same diagnostic episode, with relevant investigations and medication use recorded. For example, a study of finasteride observed a reduction in tPSA without a significant change in percent-free PSA [16]. A change in tPSA alone therefore does not establish that f/tPSA changes in the same direction.

PSAD and f/tPSA are separate predictors, but both calculations involve tPSA. They should not be assumed to be statistically independent. Model development should examine their relationship and the stability of coefficients after the additional predictor is introduced. A statistically significant regression coefficient does not necessarily mean that prediction has improved enough to alter clinical management.

AUC describes discrimination, whereas calibration assesses agreement between predicted probabilities and observed outcomes. NRI and integrated discrimination improvement (IDI) can provide additional descriptions of change, but their interpretation depends on how they are calculated and the evaluation settings. Neither establishes clinical value on its own [17]. Reporting model development, missing-data handling, and validation in accordance with TRIPOD + AI can help readers assess the reliability and applicability of the findings [18].

7. Research priorities in men aged ≥ 60 years with PSA levels in the gray zone

Existing evidence provides a rationale for investigating the incremental value of f/tPSA in men aged ≥ 60 years with tPSA levels of 4–10 ng/mL. A direct approach would use PI-RADS and PSAD in a baseline model and then add f/tPSA to construct an extended model. Both models should use the same patients, outcome definition, and validation data. If other clinical predictors are included, they should be handled consistently so that the comparison isolates the contribution of f/tPSA.

Results should be presented in terms that correspond to biopsy decisions. At a similar sensitivity for csPCa, how many additional biopsies could the extended model avoid? Alternatively, at a similar biopsy rate, could it detect more clinically significant cancers? These comparisons are more informative for clinical use than reporting a high AUC for the three-variable model alone.

Patients with negative MRI findings or PI-RADS 3 lesions are relevant groups for further analysis, provided that sample size and the number of outcome events are sufficient. An improvement in overall model performance should also be examined to determine whether the benefit is concentrated within a particular PI-RADS category. A result confined to one subgroup should not be generalized to all patients.

Study design must distinguish retrospective estimates from actual clinical implementation. Calculating the number of potentially avoidable biopsies from historical biopsy results represents a simulated decision within an existing cohort. Whether patients whose biopsies are deferred subsequently experience delayed cancer detection requires follow-up data. Guidelines allow biopsy omission to be considered in selected low-risk patients while retaining a requirement for monitoring [1]. Subsequent research should therefore assess outcomes among patients who defer biopsy, alongside model validation.

8. Conclusions

Evidence supports combining PI-RADS and PSAD to improve risk stratification in patients with PSA levels in the gray zone. The f/tPSA ratio has shown diagnostic value in some age groups and MRI-defined populations, but consistent direct evidence for its contribution beyond PI-RADS and PSAD remains limited. In men aged ≥ 60 years with gray-zone PSA levels, the relevant question is how adding f/tPSA changes risk estimates and biopsy decisions. Evaluation should consider discrimination and calibration together with biopsies avoided and clinically significant cancers missed to establish the clinical value of the three-variable approach.

Disclosure statement

The author declares no conflict of interest.

References

[1] European Association of Urology, 2026, EAU Guidelines on Prostate Cancer: Diagnostic Evaluation.

[2] Catalona W, Partin A, Slawin K, et al., 1998, Use of the Percentage of Free Prostate-Specific Antigen to Enhance Differentiation of Prostate Cancer from Benign Prostatic Disease: A Prospective Multicenter Clinical Trial. JAMA, 279(19): 1542–1547.

[3] Turkbey B, Rosenkrantz A, Haider M, et al., 2019, Prostate Imaging Reporting and Data System Version 2.1: 2019

Update of Prostate Imaging Reporting and Data System Version 2. European Urology, 76(3): 340–351.

[4] Kasivisvanathan V, Rannikko A, Borghi M, et al., 2018, MRI-Targeted or Standard Biopsy for Prostate-Cancer Diagnosis. New England Journal of Medicine, 378(19): 1767–1777.

[5] Wang S, Kozarek J, Russell R, et al., 2024, Diagnostic Performance of Prostate-Specific Antigen Density for Detecting Clinically Significant Prostate Cancer in the Era of Magnetic Resonance Imaging: A Systematic Review and Meta-Analysis. European Urology Oncology, 7(2): 189–203.

[6] Wen J, Liu W, Shen X, et al., 2024, PI-RADS v2.1 and PSAD for the Prediction of Clinically Significant Prostate Cancer Among Patients with PSA Levels of 4–10 ng/ml. Scientific Reports, 14: 6570.

[7] Haj-Mirzaian A, Burk K, Lacson R, et al., 2024, Magnetic Resonance Imaging, Clinical, and Biopsy Findings in Suspected Prostate Cancer: A Systematic Review and Meta-Analysis. JAMA Network Open, 7(3): e244258.

[8] Huang M, Lin Y, Xu A, et al., 2014, Percent Free Prostate-Specific Antigen Does Not Improve the Effectiveness of Prostate Cancer Detection in Chinese Men with a Prostate-Specific Antigen of 2.5–20.0 ng/ml: A Multicenter Study. Medical Oncology, 31(4): 925.

[9] Chen R, Xie L, Cai X, et al., 2015, Percent Free Prostate-Specific Antigen for Prostate Cancer Diagnosis in Chinese Men with a PSA of 4.0–10.0 ng/mL: Results from the Chinese Prostate Cancer Consortium. Asian Journal of Urology, 2(2): 107–113.

[10] Chen R, Huang Y, Cai X, et al., 2015, Age-Specific Cutoff Value for the Application of Percent Free Prostate-Specific Antigen (PSA) in Chinese Men with Serum PSA Levels of 4.0–10.0 ng/ml. PLoS ONE, 10(6): e0130308.

[11] Baruah S, Das N, Baruah S, et al., 2019, Combining Prostate-Specific Antigen Parameters with Prostate Imaging Reporting and Data System Score Version 2.0 to Improve Its Diagnostic Accuracy. World Journal of Oncology, 10(6): 218–225.

[12] Zhang Y, Zhu G, Zhao W, et al., 2020, A PI-RADS-Based New Nomogram for Predicting Clinically Significant Prostate Cancer: A Cohort Study. Cancer Management and Research, 12: 3631–3641.

[13] Liang Z, Feng T, Zhou Y, et al., 2024, Nomograms for Predicting Clinically Significant Prostate Cancer in Men With PI-RADS-3 Biparametric Magnetic Resonance Imaging. American Journal of Cancer Research, 14(1): 73–85.

[14] Ding Z, Wu H, Song D, et al., 2020, Development and Validation of a Nomogram for Predicting Prostate Cancer in Men with Prostate-Specific Antigen Grey Zone Based on Retrospective Analysis of Clinical and Multi-Parameter Magnetic Resonance Imaging/Transrectal Ultrasound Fusion-Derived Data. Translational Andrology and Urology, 9(5): 2179–2191.

[15] Jin P, Wang X, Ding Z, et al., 2025, Development and Validation of Risk-Stratified Biopsy Decision Pathways Incorporating MRI and PSA-Derived Indicators. Annals of Medicine, 57(1): 2446695.

[16] Pannek J, Marks L, Pearson J, et al., 1998, Influence of Finasteride on Free and Total Serum Prostate Specific Antigen Levels in Men with Benign Prostatic Hyperplasia. The Journal of Urology, 159(2): 449–453.

[17] Cook N, 2018, Quantifying the Added Value of New Biomarkers: How and How Not. Diagnostic and Prognostic Research, 2: 14.

[18] Collins G, Moons K, Dhiman P, et al., 2024, TRIPOD + AI Statement: Updated Guidance for Reporting Clinical Prediction Models That Use Regression or Machine Learning Methods. BMJ, 385: e078378.

Publisher's note

Bio-Byword Scientific Publishing remains neutral with regard to jurisdictional claims in published maps and institutional affiliations.

Urology Research, 2026, Volume 4, Issue 3
https://bbwpublisher.com/journal/UR
Online ISSN: 2981-8230
Print ISSN: 3083-4910

Identification of Key Targets for Proton Pump Inhibitors Induced Tubulointerstitial Nephritis Based on Pharmacovigilance and Network Toxicology Analysis

Haolong Li[1,2], Zhu Wang[2]*, Hui Liang[2]*

[1]Shenzhen Institutes of Advanced Technology, Chinese Academy of Sciences, Shenzhen 518055, Guangdong, China
[2]Department of Urology, The Longhua Affiliated Hospital (People's Hospital of Longhua), School of Medicine, Southern University of Science and Technology, Shenzhen 518109, Guangdong, China.

***Corresponding authors**: Hui Liang, lianghui8689@smu.edu.cn; Zhu Wang, wangzhu@smu.edu.cn

Copyright: © 2026 Author(s). This is an open-access article distributed under the terms of the Creative Commons Attribution License (CC BY 4.0), permitting distribution and reproduction in any medium, provided the original work is cited.

Abstract: *Objective*: Although previous studies have demonstrated that proton pump inhibitors (PPIs) can induce tubulointerstitial nephritis (TIN), the specific mechanism of action remains incompletely understood. *Methods*: We integrated data from Q1 2004 to Q4 2025 in the FAERS database; the associations between PPIs and TIN were quantified by four disproportionality algorithms. The potential targets for PPIs-induced TIN were identified by combining network toxicology and protein-protein interaction networks. Moreover, molecular docking between key targets and PPIs was conducted. *Results*: Five PPIs had significantly associated with TIN: lansoprazole (ROR = 49.13, 95% CI = 46.51-51.90), pantoprazole (ROR = 33.71, 95% CI = 31.73-35.82), dexlansoprazole (ROR = 32.39, 95% CI = 27.86-37.65), omeprazole (ROR = 30.12, 95% CI = 28.45-31.88), and esomeprazole (ROR = 26.77, 95% CI = 25.58-28.02). Three key targets for PPI-induced TIN were determined: CDC42, PDGFRA, and MAPK8. Among these targets, the binding between CDC42 and esomeprazole was the most stable (binding energy: -7.44 kcal/mol). *Conclusion*: These findings suggest that PPIs may trigger TIN through multi-target interactions. This study provides potential mechanistic clues and novel targets for the early warning and precise intervention of PPI-related kidney injury.

Keywords: FAERS; Proton pump inhibitors; Tubulointerstitial nephritis; Network toxicology; Key target

Online publication: October 20, 2026

1. Introduction

Tubulointerstitial nephritis (TIN) is a main cause of kidney impairment, characterized by a diverse range of etiologies. Clinically, it is generally categorized into acute and chronic forms [1]. This disease is marked by inflammation in the interstitial tubular area of the kidney, frequently associated with a swift decline in kidney

function, exhibiting a clinical trajectory akin to acute kidney injury (AKI), and representing approximately 20% of chronic kidney disease (CKD) [2,3]. Adverse reactions to medicines-particularly antibiotics, nonsteroidal anti-inflammatory drugs (NSAID), and proton pump inhibitors (PPIs)-as well as infections, are the predominant catalysts for TIN [4,5]. Drug-induced adverse reactions and infections are the primary causes of TIN, with drug-related cases (particularly those involving antibiotics, NSAID, and PPIs) accounting for over 75% of all cases [6]. Among these, PPIs—including omeprazole, esomeprazole, lansoprazole, pantoprazole, dexlansoprazole, and rabeprazole—are widely prescribed for acid-related disorders. However, despite their extensive use and established association with severe kidney outcomes (e.g., acute interstitial nephritis and acute kidney injury), the precise molecular mechanisms through which PPIs induce TIN remain poorly elucidated (Miao and Herrmann, 2023).

The FDA Adverse Event Reporting System (FAERS) database contains millions of adverse event reports linked to drugs, offering real-world clinical data and establishing itself as one of the largest pharmacovigilance databases globally [7,8]. Network toxicology methodologies provide an effective means for swiftly and efficiently elucidating the toxicological processes of drugs [9,10]. This research employed the FAERS database to conduct a systematic pharmacovigilance analysis aimed at identifying risk characteristics of TIN associated with PPIs. Subsequently, employing network toxicology methodologies, the potential targets of PPI-induced TIN were predicted. Our analysis aims to comprehensively elucidate the underlying molecular mechanisms by which PPIs induce TIN, providing scientific evidence for clinical risk prevention and targeted interventions.

2. Materials and methods

2.1. Data source and processing

Adverse drug event (ADE) data linked to drug-induced TIN, with the drug designated as the primary suspect (PS), were retrieved from the FAERS database (https://fis.fda.gov/extensions/FPD-QDE-FAERS/FPD-QDE-FAERS.html) spanning Q1 2004 through Q4 2025. The extracted datasets comprised seven standardized files: patient demographics (DEMO), adverse reaction (REAC), drug details (DRUG), patient outcomes (OUTC), report sources (RPSR), drug therapy start dates and end dates (THER), and prescribing indications (INDI) [11]. Duplicate entries were eliminated per FDA protocol, retaining the record with the latest FDA-DT when CASEIDs overlapped, and the larger PRIMARYID when both CASEID and FDA-DT matched [12]. Drug nomenclature was harmonized using RxNorm, while ADEs were classified by mapping MedDRA® (version 27.1) system organ class (SOC) and preferred terms (PT) codes to Standardized MedDRA Queries (SMQs). Personal information, event outcomes, drug indications, and drug-related data were extracted from adverse event reports linked to “TUBULOINTERSTITIAL NEPHRITIS”, eliminating reports where the indication is “TUBULOINTERSTITIAL NEPHRITIS”. The whole study design flowchart is presented in **Figure 1**.

The study was conducted in accordance with the Basic & Clinical Pharmacology & Toxicology policy for experimental and clinical studies [13].

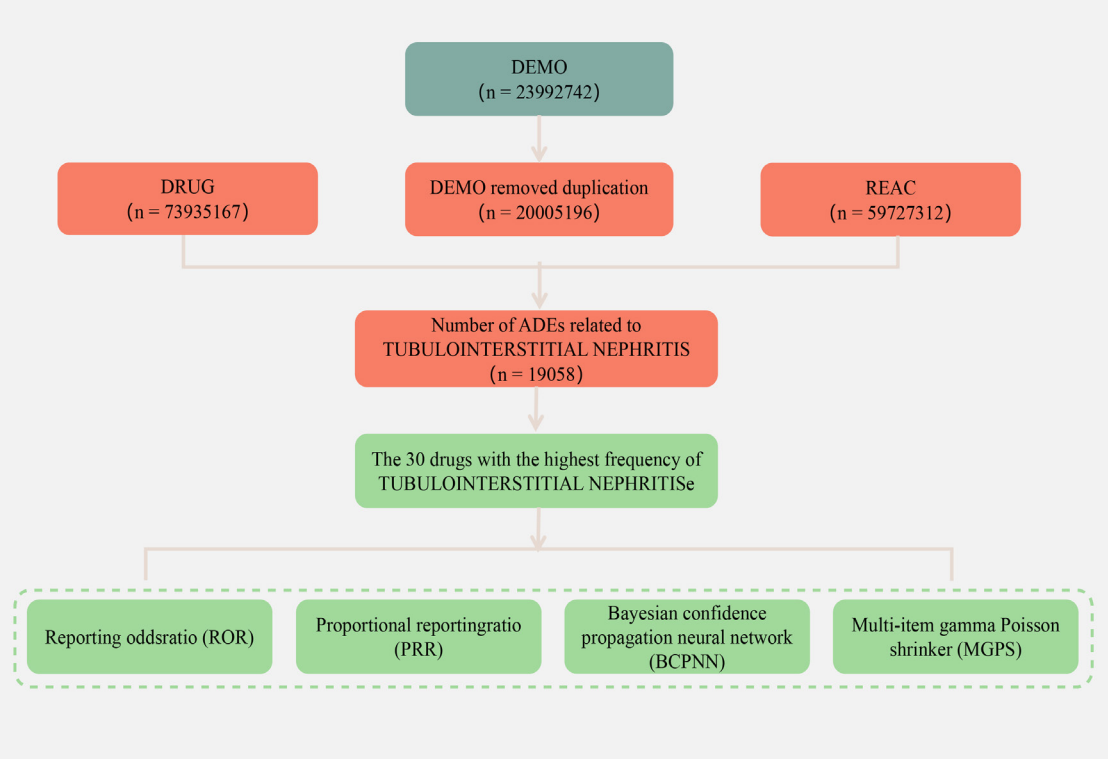


Figure 1. The flow-process diagram of tubulointerstitial nephritis (TIN) from FAERS database.

2.2. Disproportionality analysis

To evaluate potential links between TIN and pharmacological agents, four distinct disproportionality metrics were deployed: reporting odds ratio (ROR), proportional reporting ratio (PRR), Bayesian confidence propagation neural network (BCPNN), and multi-item gamma Poisson shrinker (MGPS) [14]. Each algorithm operated on a standard 2 × 2 contingency matrix. Signal detection thresholds required: minimum report count of 3, ROR lower 95% confidence interval (CI) exceeding 1, PRR ≥ 2, $\chi^2 \geq 4$, $IC_{025} > 0$, and $EBGM_{05} > 2$. Elevated ROR magnitudes suggest more pronounced associations, though such quantitative associations remain pharmacovigilance hypotheses rather than confirmed pathophysiological causation.

2.3. Target selection of drugs and TIN

For mechanistic exploration, drug-specific protein targets were computationally inferred via SwissTarget and TargetNet platforms. Disease-relevant molecular entities associated with TIN were mined from OMIM, STRING, and GENECARDS repositories using standardized disease nomenclature. The intersection of targets for both drugs and TIN was derived to pinpoint candidate genes. To investigate the functional impact and processes of candidate genes, enrichment analyses for GO and KEGG were performed utilizing the "clusterProfiler" package (version 4.6.2), with a significance threshold of adjusted $p < 0.05$ [15]. Finally, the drug-target-disease network was constructed.

2.4. Identification of key genes in TIN

A functional protein interaction map for candidate genes was generated via STRING (confidence score > 0.4). Topological prioritization leveraged six distinct centrality metrics—BottleNeck, MCC, EcCentricity, DMNC,

Degree, and ClusteringCoefficient—to extract the 20 highest-ranking nodes from each analytical framework. Genes consistently emerging across all 6 ranking schemes were designated as key genes. Subsequently, an integrative visualization depicting drug-key genes-KEGG pathways was assembled and rendered using Cytoscape.

2.5. Molecular docking

To understand the interactions of key genes with corresponding drugs, the 3D structures of drugs (SDF files) were obtained from the PubChem database (https://pubchem.ncbi.nlm.nih.gov/) and converted into PDB format using the Babel GUI. The 3D structural coordinates for proteins encoded by key genes were retrieved from the UniProt database (https://www.uniprot.org/). Prior to docking simulations, structural preprocessing—specifically elimination of crystallographic waters and dissociated low-molecular-weight ligands—was executed in AutoDock software (version 1.1.2) [16]. Then, molecular docking analysis was performed through AutoDock and visualized by PyMol.

2.6. Molecular dynamics (MD) simulation

All-atom simulations were executed in Gromacs 2022. Parameterization of ligands employed the GAFF force field, whereas macromolecular and aqueous phases were described by AMBER14SB and TIP3P, respectively. Covalent bonds involving hydrogen were constrained through the LINCS algorithm, enabling a 2-femtosecond integration timestep. Extended-range Coulombic interactions were computed via the Particle-mesh Ewald method with a 1.3-nm cutoff; van der Waals and short-range electrostatic cutoffs were set to 10 Å and updated every 10 steps. Temperature regulation at 298 K was achieved through the V-rescale thermostat, while pressure maintenance at 1 bar utilized Berendsen coupling. Following 100-ps equilibration under both NVT and NPT ensembles, a 100-nanosecond production trajectory was propagated, with atomic coordinates archived at 10-ps intervals. Trajectory post-processing and visualization leveraged VMD and PyMOL. Binding affinities were quantified through the g_mmpbsa approach. Conformational and interaction metrics—including root mean square deviation (RMSD), root mean square fluctuation (RMSF), radius of gyration (Rg), Hbond, and solvent accessible surface area (SASA)—were extracted and evaluated.

2.7. Toxicity analysis

Absorption, distribution, metabolism, excretion, and toxicity (ADMET) of compounds were profiled through the SwissADME database (http://www.swissadme.ch/). Toxicological forecasting was subsequently performed via ProTox-III database (https://tox.charite.de/protox3/).

2.8. Statistical analysis

All computational statistics were executed in R software (version 4.2.1). A *P*-value below 0.05 was considered significant.

3. Results

3.1. Descriptive characteristics

Between Q1 2004 and Q4 2025, the FAERS repository yielded 19,058 ADE records linked to TIN. **Table 1** delineated the demographic characteristics of this cohort. Regarding gender distribution, the percentage

of males (42.2%) was higher than that of females (38.8%). Age-stratified analysis revealed the highest case density within the 18-to-64-year bracket (n = 7,535, 39.5%). Most reports were submitted by physicians (n = 5,565, 29.2%), followed by other health professionals (n = 2,958, 15.5%). Outcome-wise, the dominant clinical endpoint fell under the "other serious outcomes" rubric (OT), capturing 7,302 instances or 38.3% of the total. Hospitalization (HO) (n = 6,762, 35.5%) constituted the next most frequent category. Otherwise, the top 5 reported countries of ADEs for TIN were the United States (n = 8,583, 45.0%), France (n = 1,564, 8.2%), Japan (n = 1,520, 8.0%), the United Kingdom (n = 1,260, 6.6%), and Spain (n = 682, 3.6%) **(Figure 2A)**. From 2004 to 2024, the peak of reports was in 2018 (n = 2,528, 13.3%), and the second year was 2019 (n = 2,491, 13.1%) **(Figure 2B)**.

Table 1. Clinical characteristics of patients with adverse drug events (ADEs) of tubulointerstitial nephritis (TIN)

Characteristics	Variable	Number of reports	percentage
	Overall (N = 19,058)		
Gender	Female	7,394	38.8%
	Male	8,044	42.2%
	Unknown	3,620	19.0%
Age	< 18	1,014	5.3%
	18–64	7,535	39.5%
	65–85	5,121	26.9%
	> 85	324	1.7%
	Unknown	5,064	26.6%
Reporter's occupation	Consumer (CN)	2,020	10.6%
	Health professional (HP)	2,788	14.6%
	Lawyer (LW)	1,471	7.7%
	Physician (MD)	5,565	29.2%
	Other health professional (OT)	2,958	15.5%
	Pharmacist (PH)	1,513	7.9%
	Unknown	2,742	14.4%
Reported time	2004	290	1.5%
	2005	314	1.6%
	2006	357	1.9%
	2007	341	1.8%
	2008	295	1.5%
	2009	351	1.8%
	2010	338	1.8%
	2011	371	1.9%
	2012	466	2.4%
	2013	507	2.7%
	2014	590	3.1%
	2015	467	2.5%
	2016	666	3.5%
	2017	668	3.5%
	2018	2,528	13.3%
	2019	2,491	13.1%

Characteristics	Variable	Number of reports	percentage
	2020	1,414	7.4%
	2021	1,572	8.2%
	2022	1,228	6.4%
	2023	1,300	6.8%
	2024	1,195	6.3%
	2025	1,309	6.9%
Outcome	Death (DE)	993	5.2%
	Disability (DS)	127	0.7%
	Hospitalization (HO)	6,762	35.5%
	Life -threatening (LT)	844	4.4%
	Other serious outcomes (OT)	7,302	38.3%
	Required intervention (RI)	18	0.1%
	Missing	3,009	15.8%

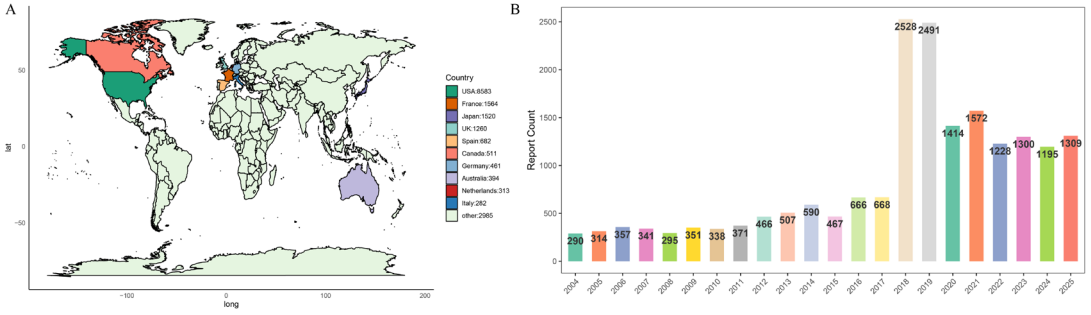


Figure 2. Signal detection for TIN. (A) Country distribution of reports for TIN. (B) Distribution of reports for TIN from 2004 to 2025.

3.2. Drug selections associated with TIN

Through pharmacovigilance signal mining, t30 pharmaceutical agents emerged as the most frequently implicated culprits in TIN pathogenesis **(Figure 3)**. These drugs included esomeprazole (n = 2,089), lansoprazole (n = 1,398), omeprazole (n = 1,276), pantoprazole (n = 1,125), and ibuprofen (n = 780). Of this prioritized pharmaceutical cohort, 27 agents exhibited statistically significant disproportionality signals, and lansoprazole had the highest interactions with TIN (ROR = 49.13 95% CI = 46.51-51.90). The rising utilization of PPIs has heightened the risk of TIN [17], promoting our focus on the drugs of PPIs: lansoprazole (ROR = 49.13, 95% CI = 46.51-51.90), pantoprazole (ROR = 33.71, 95% CI = 31.73-35.82), dexlansoprazole (ROR = 32.39, 95% CI = 27.86-37.65), omeprazole (ROR = 30.12, 95% CI = 28.45-31.88), and esomeprazole (ROR = 26.77, 95% CI = 25.58-28.02), which were also the top 5 drugs with positive signals and the higher ROR value for subsequent analysis.

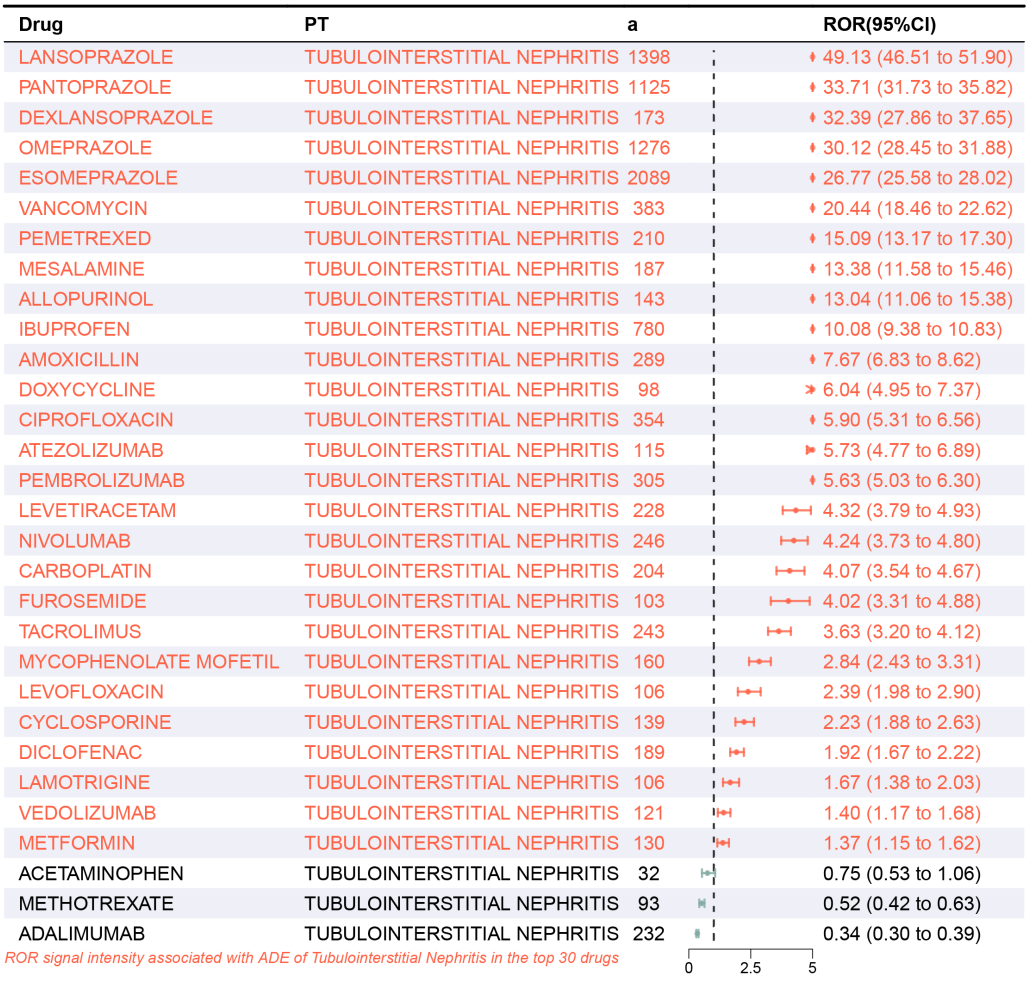


Figure 3. The forest plot for top 30 drugs caused TIN.

3.3. Pharmacological properties of PPIs

In silico ADMET characterization of the five prioritized compounds was undertaken to profile their biopharmaceutical attributes. Tabulated data reveal pronounced intestinal permeability coupled with negligible blood-brain barrier penetration, implying restricted central nervous system distribution. Additionally, each agent exhibited P-glycoprotein substrate liability alongside inhibitory potential against major hepatic CYP isoforms, notably CYP1A2, CYP2C19, CYP2D6, and CYP3A4. The log Kp value of these drugs ranged from -6.42 cm/s to -6.96 cm/s. Additionally, the toxicity of these drugs was also explored, and their predicted lethal dose (LD) was 1,400 mg/kg, and the toxicity class was 4, which indicated that these drugs were moderately toxic.

3.4. Identification and function prediction of shared targets between drugs and TIN

After summarizing and removing duplication, 252 drug-related targets and 1,024 TIN-related targets were obtained from the corresponding databases. The intersection of these targets yielded 44 candidate genes **(Figure 4A)**. To explore the functions of these candidate genes in disease, enrichment analyses were

conducted, revealing 1,325 GO terms, including phosphatidylinositol 3-kinase (PI3K)/protein kinase B (PKB) signal transduction, membrane raft, and protein tyrosine kinase activity, and 141 KEGG pathways such as AGE-RAGE signaling pathway in diabetic complications and Endocrine resistance **(Figure 4B)**. Furthermore, PPI network of candidate genes was developed with 44 nodes and 390 interaction pairs **(Figure 4C)**. Among this network, AKT1 had the most correlations with other genes, such as SIRT1, MAPK1, and PDGFRA. Additionally, a candidate gene-drug-TIN regulatory network was established with 50 nodes and 163 edges. In this network, five drugs targeted ATP4A, DNMT1, FYN, HNF4A, S1PR2, TEK, and TLR9 **(Figure 4D)**.

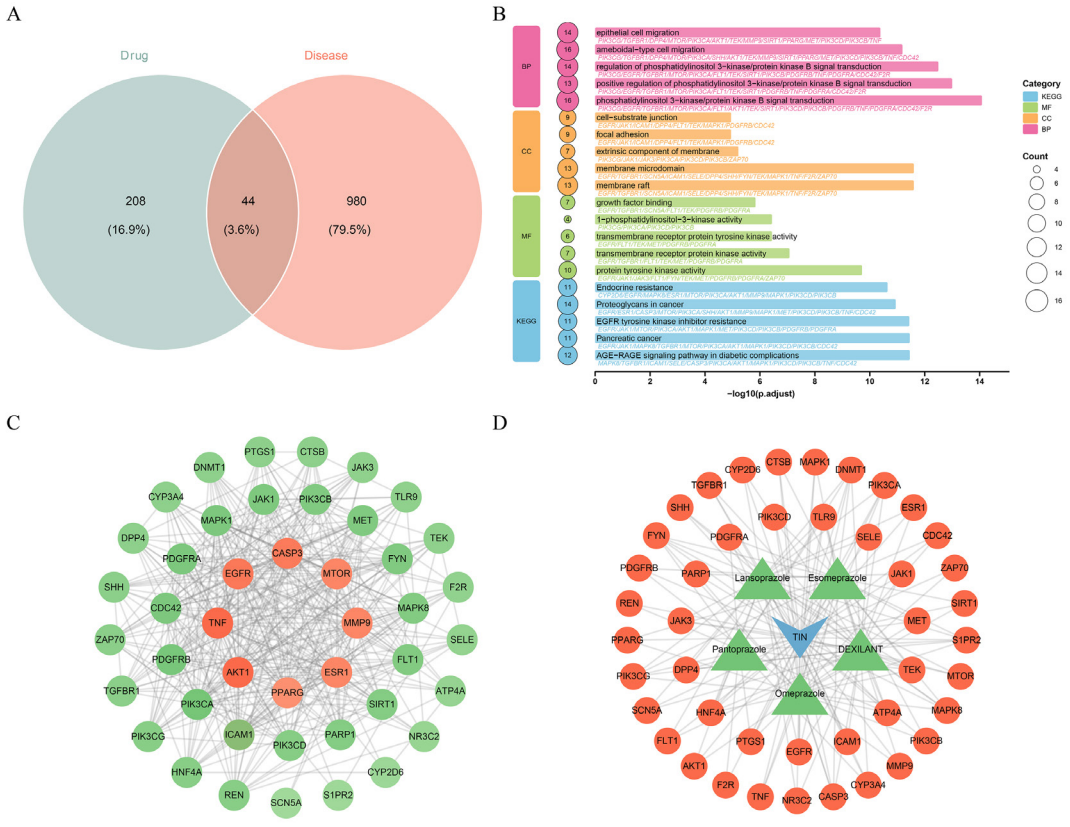


Figure 4. Identification of candidate genes in TIN. (A) The intersection of drugs and TIN-related targets. (B) The enrichment analysis of candidate genes. (C) The interactions of candidate genes at the protein level. (D) The regulatory network of candidate gene-drug-TIN. Green represents drugs; orange denotes candidate genes.

3.5. CDC42, PDGFRA, and MAPK8 were identified as key genes in TIN

Topological prioritization of the candidate gene interactome employed 6 centrality metrics—BottleNeck, MCC, EcCentricity, DMNC, Degree, and ClusteringCoefficient—to extract the 20 foremost nodes per algorithm. The convergent subset across all 6 ranking schemes comprised 3 consensus molecules: CDC42, PDGFRA, and MAPK8, designated as the key genes **(Figure 5A)**. Leveraging these pivotal targets, an integrative tripartite network was assembled, encompassing 96 vertices and 119 connections, linking pharmaceutical agents, key genes, and KEGG-annotated pathways **(Figure 5B)**. Within this architecture, omeprazole and esomeprazole converged upon PDGFRA and MAPK8, both implicated in focal adhesion

dynamics. Lansoprazole, meanwhile, engaged MAPK8 within the T-cell receptor signaling cascade. Subsequent in silico binding simulations between these core genes and their respective ligands yielded favorable thermodynamic profiles, with all affinity estimates falling below −5 kcal/mol **(Table 2)**. As shown in **Figure 5C**, omeprazole and esomeprazole correlated with CDC42 residues ALA-159, ASP-118, and GLN-116. Lansoprazole was associated with MAPK8 residues CYS-245, LEU-241, and GLY-242; omeprazole with residues ASN-114, ILE-32, and MET-111; esomeprazole with residues MET-111 and LYS-55; while dexlansoprazole with residues LEU123 and MET-218. Furthermore, omeprazole correlated with PDGFRA residues LEU-599 and ASP-681; pantoprazole with PDGFRA residues ARG-558 and ARG-554; while esomeprazole correlated with residues GLN-619, TYR-676, and LYS-623.

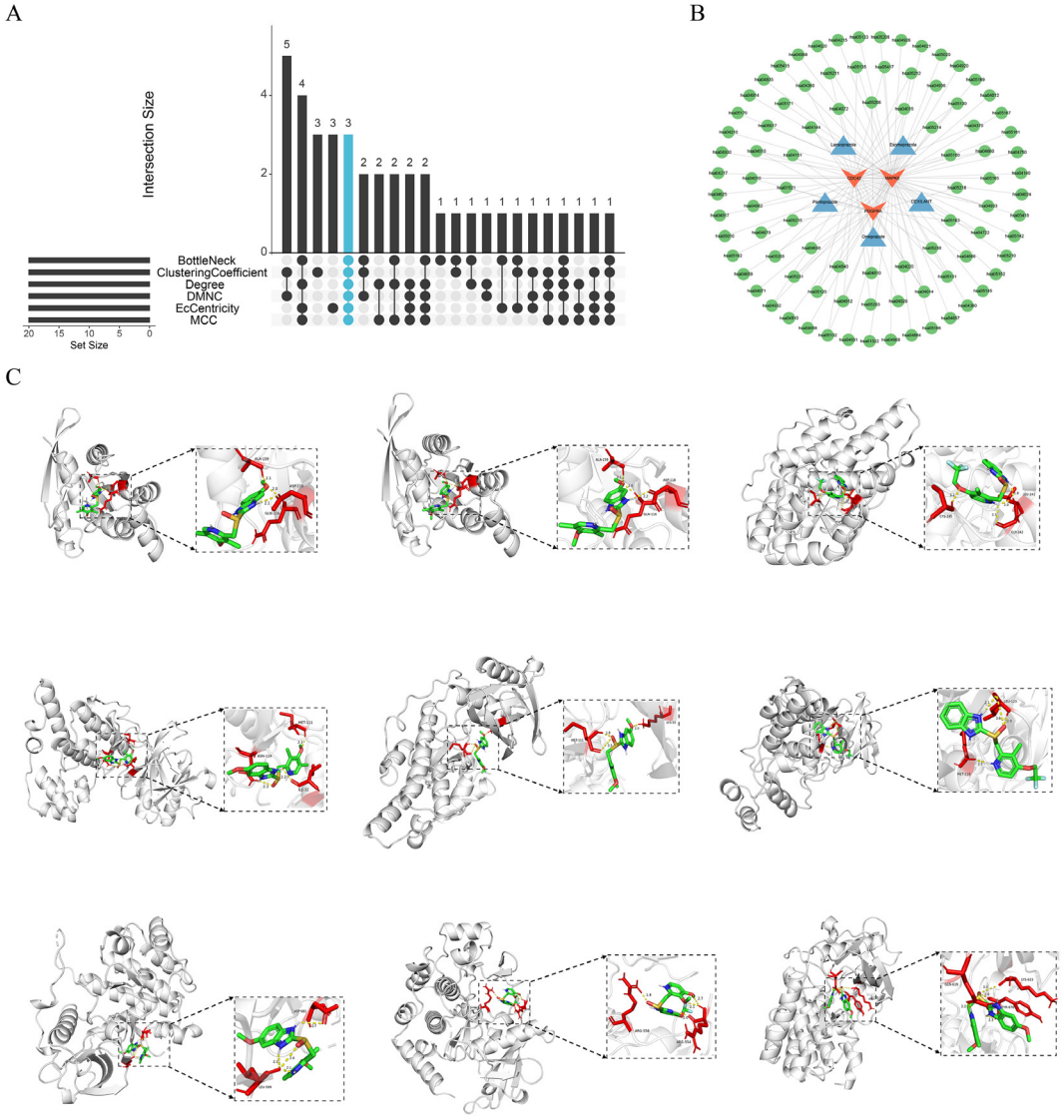


Figure 5. CDC42, PDGFRA, and MAPK8 were identified as key genes in TIN. **(A)** The selection of key genes by 6 algorithms. **(B)** The regulatory network of drug-key gene-pathway. Orange represents key genes, blue denotes drug, and green represents pathways. **(C)** Molecular docking analysis between drugs with key genes.

Table 2. The molecular docking of key genes with drugs

Key genes	UniProt	PDB	Drugs	CID	Binding energy (kcal/mol)	Number of hydrogen
CDC42	P60953	1AN0	Omeprazole	CID4594	-7.335	3
CDC42	P60953	1AN0	Esomeprazole	CID9568614	-7.44	3
MAPK8	P45983	2XS0	Lansoprazole	CID3883	-5.53	4
MAPK8	P45983	2XS0	Omeprazole	CID4594	-6.1	3
MAPK8	P45983	2XS0	Esomeprazole	CID9568614	-7.15	3
MAPK8	P45983	2XS0	Dexlansoprazole	CID9578005	-5.88	4
PDGFRA	P16234	8PQJ	Omeprazole	CID4594	-6.99	4
PDGFRA	P16234	8PQJ	Pantoprazole	CID4679	-6.06	4
PDGFRA	P16234	8PQJ	Esomeprazole	CID9568614	-6.72	4

3.6. CDC42-esomeprazole compound had a stable structure

Collectively, these orthogonal lines of evidence affirm a robust and stable CDC42–esomeprazole interaction.

Tabulated data in **Table 2** identified the CDC42-esomeprazole pairing as exhibiting the most favorable thermodynamic signature (-7.44 kcal/mol), prompting MD simulation of this complex. Trajectory interrogation across the 100-ns production run evidenced structural equilibration, as gauged by RMSD, RMSF, and Rg **(Figure 6A-C)**. Intermolecular hydrogen-bond occupancy oscillated between zero and four throughout the simulation window **(Figure 6D)**. The SASA variability reflected ongoing conformational sampling; notably, Buried SASA remained non-0, signifying persistent interfacial contact and complex integrity **(Figure 6E)**. Finally, their ΔE_{MMPBSA} value was -80.026 ± 10.403 kJ/mol, corroborating pronounced ligand–receptor affinity. Collectively, these orthogonal lines of evidence affirm a robust and stable CDC42–esomeprazole interaction.

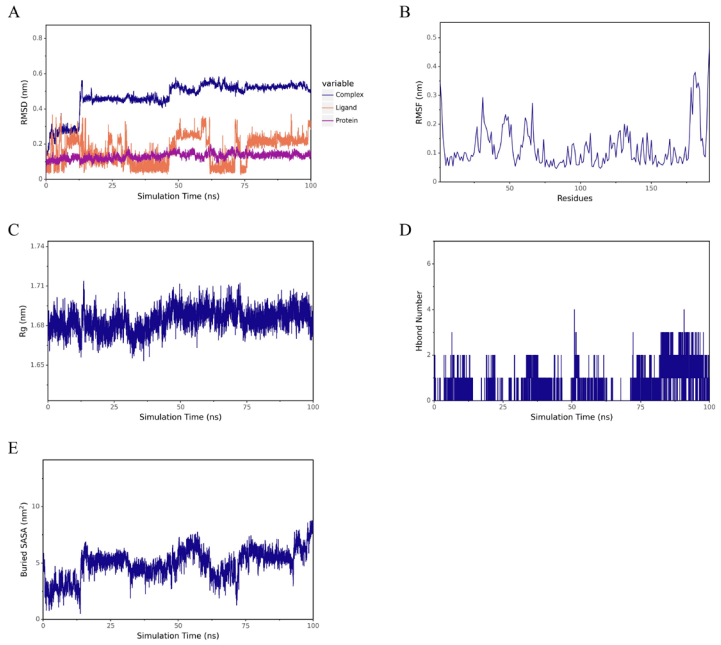


Figure 6. Molecular dynamics analysis of CDC42-esomeprazole compound. **(A-C)** The results of root mean square deviation (RMSD) (A), root mean square fluctuation (RMSF) (B), and radius of gyration (Rg) (C) for the CDC42-esomeprazole compound. (D) The number of H-bonds. (E) The Buried solvent accessible surface area (SASA) result.

4. Discussion

Previous studies indicate a substantial correlation between PPIs and kidney illnesses such as AKI and CKD [18]. Hart E *et al.* discovered that PPIs can elevate the chance of AKI development by as much as sixfold, while Al-Aly Z *et al.* established a robust correlation between PPI use and heightened risk of CKD initiation and progression [19]. In this study, five PPI drugs showed the strongest association with TIN: lansoprazole (ROR = 49.13, 95% CI = 46.51–51.90), pantoprazole (ROR = 33.71, 95% CI = 31.73–35.82), dexlansoprazole (ROR = 32.39, 95% CI = 27.86–37.65), omeprazole (ROR = 30.12, 95% CI = 28.45–31.88), and esomeprazole (ROR = 26.77, 95% CI = 25.58–28.02). Among these drugs, omeprazole was found to induce oxidative stress and apoptosis in kidney tubular cells via mechanisms including membrane-associated protein V/7-AAD staining, LDH release, abnormal chromatin condensation, and vesicle formation, resulting in kidney injury [20]. Lansoprazole, specially, influences regulatory mechanisms in AIN by altering T-cell immunological responses [21]. At present, there is inadequate evidence about the role of alternative drugs in TIN. Nonetheless, current research indicates that PPIs can activate host immune responses via semi-antigenisation (by binding to larger host proteins to gain immunogenicity) or through direct interactions with immune receptors or major histocompatibility complex (MHC) proteins (pharmacological interactions) [22]. The accumulation of PPIs and their metabolites in interstitial spaces, together with subsequent immunological reactions, may be potential underlying causes of the illness [23]. Lesions in the tubulointerstitium can precipitate a swift decline in kidney function and exacerbate AKI, attributed to chronic interstitial nephritis (CIN), finally culminating in kidney failure and, in severe instances, CKD [24]. These findings further confirm that PPIs are not only associated with kidney injury in a broad sense, but also that their specific risk of inducing TIN varies between drugs and may drive disease progression through shared immune-inflammatory pathways.

Subsequently, network toxicology analysis further identified three potential targets (CDC42, PDGFRA, and MAPK8) for PPI-induced TIN. Existing research indicates that these three targets are involved in regulating crucial pathophysiological processes, including cytoskeletal reorganization and tubular morphogenesis, tissue repair and fibrosis progression, as well as inflammatory responses and apoptosis, thereby playing pivotal roles in renal injury. Specifically, the ablation of CDC42 markedly diminishes the expression of α-SMA, fibronectin, and type I collagen in kidney fibroblasts, concurrently inhibiting the pathways that facilitate fibroblast activation [25]. Recent findings indicate that CDC42 is predominantly expressed in kidney tubules and the kidney tubular interstitium, significantly influencing kidney tubule formation through the regulation of cytoskeletal dynamics. Inhibition of CDC42 markedly reduces kidney tubular injury, encompassing significant vacuolization, granular degeneration, epithelial cell flattening, and lumen dilatation [26]. In the study by Toda N *et al.,* PDGFRA was shown to be expressed in multiple renal cell types, including collecting duct cells, proximal tubular cells, and interstitial fibroblasts [27]. Moreover, in CKD mice, hedgehog signaling was observed to enhance PDGFRA expression and promote the development of new endothelium in arteriovenous fistulas [28]. In ischemia-reperfusion-induced acute kidney damage, MAPK8 is markedly activated in kidney tissue, and the inhibition of MAPK8 diminishes tubular necrosis and inflammatory infiltration [29]. Furthermore, Bruno S *et al.* discovered that the activation of the MAPK8-mediated pathway is involved in both G2/M arrest and apoptosis of kidney tubular epithelial cells, while also enhancing the expression of TGF-β1 and CTGF in G2/M-arrested kidney tubular cells. These results in aberrant repair of kidney tubular epithelial cells, increased collagen production, and the facilitation of fibrosis progression [30,31]. However, the specific molecular pathways by which PPIs act on these targets to initiate

immune-inflammatory responses and cause tubulointerstitial injury remain unclear. Future experimental investigations are required to better substantiate the regulatory functions of these targets and their upstream and downstream signaling networks in PPI-associated TIN, thereby providing more direct evidence for elucidating its pathogenic mechanisms.

In silico binding predictions between the prioritized gene set and corresponding ligands identified the CDC42–esomeprazole association as the most thermodynamically favorable, registering a minimum affinity estimate of −7.44 kcal/mol. This optimal complex was subsequently advanced to explicit-solvent molecular dynamics. MD analysis—encompassing RMSD, RMSF, and Rg—corroborated sustained conformational integrity throughout the simulated interval. Esomeprazole is a type of PPI that can be efficiently utilized in the clinical management of peptic ulcers and associated conditions, providing benefits such as enhanced metabolic stability and increased bioavailability [32]. This interaction provides structural evidence for understanding how PPIs disrupt cytoskeletal regulation through specific molecular interactions, potentially driving renal tubulointerstitial injury. Molecular dynamics simulations reveal the dynamic behavior of protein-drug complexes at the atomic level, aiding in elucidating the potential origins of PPI-related nephrotoxicity at the mechanistic level [33].

By integrating the FAERS database with network toxicology, this study for the first time systematically identified potential molecular targets (CDC42, PDGFRA, and MAPK8) for PPI-induced TIN, thereby advancing the mechanistic understanding of PPI-related nephrotoxicity and offering new leads for targeted intervention. Nonetheless, our study possesses specific limitations. Reports submitted to FAERS are voluntary in nature, which introduces inherent limitations including incomplete capture of adverse events, temporal lags in documentation, and information gaps. Moreover, investigations leveraging this pharmacovigilance repository for safety profiling remain observational in design, thereby precluding the establishment of definitive causality between the investigated therapeutic agents and TIN. Ultimately, although network pharmacology and bioinformatics investigations have pinpointed key targets for PPI-induced TIN, the specific pathogenic mechanisms remain to be fully elucidated. Subsequent basic experiments are required to validate these key targets and further clarify the specific pathogenic mechanisms of PPI-related TIN.

5. Conclusion

This study further substantiates the high correlation between PPIs and TIN through FAERS database, revealing differential risks among different PPI drugs, particularly lansoprazole. By integrating network toxicology and molecular docking simulations, the study systematically identified potential key targets such as CDC42, PDGFRA, and MAPK8 for the first time, providing new directions for elucidating the molecular mechanisms underlying PPI-induced TIN. These findings suggest that clinical practice should strengthen early renal function monitoring during PPI use, particularly for high-risk formulations, and lay a theoretical foundation for developing targeted intervention strategies. Despite inherent limitations of spontaneous reporting databases, the multidimensional analytical approach provides crucial insights for understanding the mechanisms and prevention of drug-induced kidney injury.

Data availability statement

Adverse drug events (ADEs) data used in this study were downloaded from the FAERS database (https://

www.fda.gov/drugs).

Funding

Medical Scientific Research Foundation of Guangdong Province (Project No.: B2025219, HLL); Medical research project of Shenzhen Longhua Medical Association (Project No.: 2023LHMA01, ZW); Construction Funds of Key Clinical Medical Disciplines in Longhua District, Shenzhen (Project No.: MKD202508210305, HL)

Disclosure statement

The authors declare no conflict of interest.

References

[1] Hyodo T, Hara S, Goto S, et al., 2024, Immunohistological Analysis Reveals IgG1-Dominant Immunophenotype of Tubulointerstitial Nephritis Unassociated with IgG4-Related Diseases. International Urology and Nephrology, 56(7): 2363–2369.

[2] Sahutoglu T, Perazella M, 2025, Update on Acute Tubulointerstitial Nephritis: Clinical Features, Immunologic Insights, and Diagnostic and Treatment Approaches. Kidney International Reports, 10(6): 1643–1656.

[3] Pan X, Guo Z, Zheng Y, et al., 2025, Effects of Fourteen Essential Minerals and Vitamins on Acute and Chronic Tubulointerstitial Nephritis: A Multivariate Mendelian Randomization Study. Hereditas, 162(1): 63.

[4] Ho H, Shirakawa H, 2022, Oxidative Stress and Mitochondrial Dysfunction in Chronic Kidney Disease. Cells, 12(1): 88.

[5] Standardization of Uveitis Nomenclature (SUN) Working Group, 2021, Classification Criteria for Tubulointerstitial Nephritis with Uveitis Syndrome. American Journal of Ophthalmology, 228: 255–261.

[6] Torigoe K, Yoshida Y, Sakamoto R, et al., 2023, Improvement in Tubulointerstitial Nephritis with Glucocorticoid Therapy in an Anorexia Nervosa Patient. Journal of Medical Cases, 14(9–10): 344–349.

[7] Yin Y, Shu Y, Zhu J, et al., 2022, A Real-World Pharmacovigilance Study of FDA Adverse Event Reporting System (FAERS) Events for Osimertinib. Scientific Reports, 12(1): 19555.

[8] Horinouchi Y, Ikeda Y, Fukushima K, et al., 2018, Renoprotective Effects of a Factor Xa Inhibitor: Fusion of Basic Research and a Database Analysis. Scientific Reports, 8(1): 10858.

[9] Huang S, 2023, Efficient Analysis of Toxicity and Mechanisms of Environmental Pollutants with Network Toxicology and Molecular Docking Strategy: Acetyl Tributyl Citrate as an Example. Science of the Total Environment, 905: 167904.

[10] Zhao Z, Du J, Wang Q, et al., 2023, An Integrated Strategy Combining Network Toxicology and Feature-Based Molecular Networking for Exploring Hepatotoxic Constituents and Mechanism of Epimedii Folium-Induced Hepatotoxicity In Vitro. Food and Chemical Toxicology, 176: 113785.

[11] Zhang L, Mao W, Liu D, et al., 2023, Risk Factors for Drug-Related Acute Pancreatitis: An Analysis of the FDA Adverse Event Reporting System (FAERS). Frontiers in Pharmacology, 14: 1231320.

[12] Wang J, Zhang Z, Liu X, et al., 2024, Exploring Novel Adverse Events of Nefecon. Kidney International Reports, 9(9): 2705–2717.

[13] Tveden-Nyborg P, Bergmann T, Jessen N, et al., 2025, BCPT 2026 Policy for Experimental and Clinical Studies.

Basic & Clinical Pharmacology & Toxicology, 137(6): e70159.

[14] Jiang Y, Zhou L, Shen Y, et al., 2024, Safety Assessment of Brexpiprazole: Real-World Adverse Event Analysis from the FAERS Database. Journal of Affective Disorders, 346: 223–229.

[15] Yu G, Wang L, Han Y, et al., 2012, clusterProfiler: An R Package for Comparing Biological Themes Among Gene Clusters. Omics, 16(5): 284–287.

[16] Trott O, Olson A, 2010, AutoDock Vina: Improving the Speed and Accuracy of Docking with a New Scoring Function, Efficient Optimization, and Multithreading. Journal of Computational Chemistry, 31(2): 455–461.

[17] Blank M, Parkin L, Paul C, et al., 2014, A Nationwide Nested Case-Control Study Indicates an Increased Risk of Acute Interstitial Nephritis with Proton Pump Inhibitor Use. Kidney International, 86(4): 837–844.

[18] Luo H, Yi G, Tang H, et al., 2024, Proton Pump Inhibitors May Increase the Risk of Cisplatin-Induced Acute Kidney Injury in Patients with Nasopharyngeal Carcinoma: A Prospective Cohort Study. Scientific Reports, 14(1): 18839.

[19] Al-Aly Z, Maddukuri G, Xie Y, 2020, Proton Pump Inhibitors and the Kidney: Implications of Current Evidence for Clinical Practice and When and How to Deprescribe. American Journal of Kidney Diseases, 75(4): 497–507.

[20] Fontecha-Barriuso M, Martín-Sanchez D, Martinez-Moreno J, et al., 2020, Molecular Pathways Driving Omeprazole Nephrotoxicity. Redox Biology, 32: 101464.

[21] Koda R, Watanabe H, Tsuchida M, et al., 2018, Immune Checkpoint Inhibitor (Nivolumab)-Associated Kidney Injury and the Importance of Recognizing Concomitant Medications Known to Cause Acute Tubulointerstitial Nephritis: A Case Report. BMC Nephrology, 19(1): 48.

[22] Raghavan R, Shawar S, 2017, Mechanisms of Drug-Induced Interstitial Nephritis. Advances in Chronic Kidney Disease, 24(2): 64–71.

[23] Parmar M, Kaleem S, Samuganathan P, et al., 2023, Impact of Proton Pump Inhibitors on Kidney Function and Chronic Kidney Disease Progression: A Systematic Review. Cureus, 15(12): e49883.

[24] Targownik L, Fisher D, Saini S, 2022, AGA Clinical Practice Update on De-Prescribing of Proton Pump Inhibitors: Expert Review. Gastroenterology, 162(4): 1334–1342.

[25] Hu X, Gan L, Tang Z, et al., 2024, A Natural Small Molecule Mitigates Kidney Fibrosis by Targeting Cdc42-Mediated GSK-3β/β-Catenin Signaling. Advanced Science (Weinh), 11(13): e2307850.

[26] Zhang Q, Qin Z, Wang Q, et al., 2024, Pharmacokinetic Profiling of ZCL-278, a Cdc42 Inhibitor, and Its Effectiveness Against Chronic Kidney Disease. Biomedicine & Pharmacotherapy, 179: 117329.

[27] Toda N, Mori K, Kasahara M, et al., 2017, Crucial Role of Mesangial Cell-Derived Connective Tissue Growth Factor in a Mouse Model of Anti-Glomerular Basement Membrane Glomerulonephritis. Scientific Reports, 7: 42114.

[28] Song K, Qing Y, Guo Q, et al., 2020, PDGFRA in Vascular Adventitial MSCs Promotes Neointima Formation in Arteriovenous Fistula in Chronic Kidney Disease. JCI Insight, 5(21): e137298.

[29] Kanellis J, Ma F, Kandane-Rathnayake R, et al., 2010, JNK Signaling in Human and Experimental Renal Ischaemia/Reperfusion Injury. Nephrology Dialysis Transplantation, 25(9): 2898–2908.

[30] Bruno S, Tapparo M, Collino F, et al., 2017, Renal Regenerative Potential of Different Extracellular Vesicle Populations Derived from Bone Marrow Mesenchymal Stromal Cells. Tissue Engineering Part A, 23(21–22): 1262–1273.

[31] Ma M, Luo Q, Fan L, et al., 2022, The Urinary Exosomes Derived from Premature Infants Attenuate Cisplatin-Induced Acute Kidney Injury in Mice via MicroRNA-30a-5p/Mitogen-Activated Protein Kinase 8 (MAPK8).

Bioengineered, 13(1): 1650–1665.

[32] Borekci A, Kuru Bektasoglu P, Somay A, et al., 2025, Esomeprazole's Antifibrotic Effects on Rats with Epidural Fibrosis. Global Spine Journal, 15(5): 2611–2616.

[33] Hollingsworth S, Dror R, 2018, Molecular Dynamics Simulation for All. Neuron, 99(6): 1129–1143.

Publisher's note

Bio-Byword Scientific Publishing remains neutral with regard to jurisdictional claims in published maps and institutional affiliations.

Urology Research, 2026, Volume 4, Issue 3
https://bbwpublisher.com/journal/UR
Online ISSN: 2981-8230
Print ISSN: 3083-4910

Application of Distal Urethral Mobilization in the Duckett Procedure for Hypospadias

Yi Wang, Shuai Han, Linlin Fan, Liwei Li

Baoding Hospital of Beijing Children's Hospital, Capital Medical University, Baoding 071000, Hebei, China

Copyright: © 2026 Author(s). This is an open-access article distributed under the terms of the Creative Commons Attribution License (CC BY 4.0), permitting distribution and reproduction in any medium, provided the original work is cited.

Abstract: *Objective*: To investigate the value of distal urethral mobilization in the Duckett procedure. *Methods*: A retrospective analysis was conducted on 96 children with hypospadias treated between January 2017 and June 2023. Patients were divided into an observation group (52 cases) and a control group (44 cases) based on whether distal urethral mobilization was performed intraoperatively. The neourethral length, operative time, postoperative complications, maximum urinary flow rate (Qmax), and HOSE scores were compared between the two groups. *Results*: The neourethral length in the observation group was shorter than that in the control group [(2.4 ± 0.6) cm vs. (3.3 ± 0.7) cm, $p < 0.001$], while operative time was comparable between the two groups ($p = 0.077$). The overall complication rate [21.2% vs. 59.1%], urethrocutaneous fistula rate [9.6% vs. 25.0%], and reoperation rate [7.7% vs. 27.3%] were all lower in the observation group than in the control group ($p < 0.001$, 0.044, 0.010). Among those followed up for at least 12 months, the observation group demonstrated superior Qmax [(13.1 ± 2.9) mL/s vs. (11.4 ± 3.0) mL/s] and HOSE scores [(15.2 ± 1.4) vs. (13.8 ± 2.1)] compared with the control group ($p = 0.020$, $p < 0.001$). Conclusion This technique shortens the neourethral length, reduces the risk of urethrocutaneous fistula and reoperation, and improves midterm voiding function.

Keywords: Hypospadias; Duckett procedure; Distal urethral mobilization; Urethral plate; Urethrocutaneous fistula; Children

Online publication: October 20, 2026

1. Introduction

Hypospadias is one of the most common congenital genitourinary malformations in boys, with an incidence ranging from 1 in 300 to 1 in 200 live male births [1]. More than 300 surgical techniques have been documented, yet none is universally applicable to all anatomical variants [2]. The Expert Consensus on Hypospadias states that the recognized incidence of urethrocutaneous fistula ranges from 15% to 30% [3]. The transverse preputial island flap urethroplasty (Duckett procedure) is the mainstream technique for moderate to severe hypospadias in China; however, postoperative complications have not declined in parallel with the dissemination of the technique [4]. Flap length and urethral defect length are associated with short-term

complications [5]. A single-center study of 136 cases reported incidences of urethrocutaneous fistula, stricture, and diverticulum after one-stage Duckett procedure of 17.6%, 12.5%, and 8.1%, respectively [6].

Morphological studies have shown that scattered corpus spongiosum tissue surrounding the urethral plate possesses considerable blood supply, and the degree of abnormality correlates positively with hypospadias severity [7]. However, urethral plate-preserving techniques are only suitable for distal and mid-penile cases without or with mild curvature; those with longer urethral defects still require transection of the urethral plate. Urethral mobilization and advancement follows the approach of preserving autologous urethra. Edan reported 65 cases of distal hypospadias with no urethrocutaneous fistula during follow-up and a stricture rate of 4.6% [8]. This study introduces this concept into the Duckett procedure: before transecting the urethral plate, the dysplastic urethra distal to the meatus is mobilized en bloc together with the underlying spongiosum-like tissue, gaining space to extend toward the glans and thereby shortening the length of urethra requiring replacement by a tube.

2. Materials and methods

2.1. General information

2.1.1. Inclusion criteria

(1) First urethroplasty;
(2) Meatal location at the penile shaft to penoscrotal junction after curvature correction;
(3) Sufficient dorsal preputial skin for harvesting a transverse island flap;
(4) Follow-up of at least 6 months.

2.1.2. Exclusion criteria

(1) History of prior urethroplasty or fistula repair;
(2) Concomitant micropenis, cryptorchidism,or disorders of sex development;
(3) Intraoperative assessment indicating the need for staged surgery.

According to the above criteria,96 children who underwent the Duckett procedure at our hospital between January 2017 and June 2023 were included and divided into an observation group (52 cases) and a control group (44 cases) based on whether distal urethral mobilization was performed. Age, preoperative curvature angle, and hypospadias type did not differ significantly between the two groups ($p > 0.05$), as shown in **Table 1**. This study was approved by the hospital ethics committee (2023-KY-036).

Table 1. Comparison of general data between the two groups

Parameter	Observation group (n = 52)	Control group (n = 44)	t/χ^2	p
Age (years, $\overline{x} \pm s$)	3.2 ± 1.1	3.5 ± 1.3	1.24	0.218
Preoperative curvature angle (°, $\overline{x} \pm s$)	26.4 ± 7.2	27.8 ± 7.6	0.94	0.350
Penile shaft type [n (%)]	31 (59.6)	26 (59.1)	0.06	0.970
Penoscrotal and scrotal type [n (%)]	21 (40.4)	18 (40.9)		

2.2. Surgical methods

All procedures were performed by the same surgical team under endotracheal general anesthesia combined with caudal block. The patient was placed in the supine position, and a 4-0 silk traction suture was placed

through the glans. A circumferential incision was made 0.5–0.8 cm from the coronal sulcus, with a U-shaped ventral extension around the proximal margin of the meatus down to the tunica albuginea. Degloving was performed superficial to Buck's fascia toward the penile base. After excision of ventral fibrous bands, an artificial erection test was performed; residual curvature exceeding 30° was corrected by dorsal tunica albuginea plication.

Distal urethral mobilization (observation group): Longitudinal incisions were made on both sides of the meatus along the junction between the urethral plate and the glans wings, extending through the mucosa to the surface of the tunica albuginea. Using fine scissors, sharp dissection was performed in the plane between the deep surface of the urethral plate and the tunica albuginea, mobilizing the urethra en bloc together with the underlying spongiosum-like tissue into the glans spongiosum, while preserving 2–3 mm of tissue on each side of the urethral plate. After mobilization, the distal urethra was grasped and advanced toward the glans to confirm absence of tension, and the proximal end of the mobilized segment was trimmed obliquely. In this group, the distal urethra was advanced by 0.5–1.6 cm, with a mean of (0.9 ± 0.3) cm. In the control group, the urethral plate and distal fibrous bands were transected according to the original Duckett technique.

Flap harvest and tubularization: The dorsal preputial inner plate was retracted at four corners to form a rectangle. The flap length was designed as the distance from the meatus to the glans tip plus 0.5 cm, with a width of 1.2 cm (< 3 years) or 1.5 cm (≥ 3 years). The vascular pedicle was dissected to the penile base, with a pedicle width no less than the flap width. The flap was tubularized over an 8–10 F silicone stent using continuous inverting sutures with 6-0 absorbable suture. The proximal end was anastomosed end-to-end to the obliquely trimmed mobilized distal urethra (or the native meatus in the control group). The distal end was brought through a glans tunnel to the glans tip to create a slit-like meatus. A dorsal pedicled dartos flap was used to cover the suture line and anastomosis.

2.3. Postoperative management and follow-up

Prophylactic second-generation cephalosporins were administered until stent removal. The dressing was removed at 5–7 days, and the stent was removed at 10–14 days. Voiding stream, caliber, and any leakage were observed. Follow-up visits were scheduled at 1, 3, 6, and 12 months postoperatively, and annually thereafter. Urethrocutaneous fistula was defined as the presence of an ectopic voiding channel after stent removal. Urethral stricture was defined as a narrowed stream or voiding difficulty confirmed by calibration or urethrography. Urethral diverticulum was determined by ventral bulging during voiding combined with ultrasonography.

2.4. Outcome measures and statistical methods

The primary outcome was the incidence of urethrocutaneous fistula within 6 months postoperatively. Secondary outcomes included urethral stricture, urethral diverticulum, wound infection, reoperation rate, neourethral length, operative time, and time to stent removal. Patients followed for at least 12 months who were able to cooperate underwent uroflowmetry, and the Hypospadias Objective Scoring Evaluation (HOSE, maximum 16 points) was used to assess meatal location and shape, urinary stream, erectile morphology, and presence of fistula. SPSS 26.0 software was used. Continuous data were expressed as $\overline{x} \pm s$ and compared using independent-samples *t*-tests. Categorical data were expressed as n (%) and compared using the χ^2 test; Fisher's exact test was used when expected frequencies were < 5. $p < 0.05$ was considered statistically significant.

3. Results

3.1. Intraoperative and early postoperative parameters

The neourethral length in the observation group was shorter than that in the control group ($p < 0.001$), while operative time did not differ significantly between the two groups ($p > 0.05$), as shown in **Table 2**.

Table 2. Comparison of intraoperative parameters between the two groups ($\overline{x} \pm s$)

Parameter	Observation group (n = 52)	Control group (n = 44)	*t*	*p*
Neourethral length (cm)	2.4 ± 0.6	3.3 ± 0.7	6.78	< 0.001
Operative time(min)	102.6 ± 18.1	96.3 ± 16.9	1.79	0.077

3.2. Postoperative complications

The overall complication rate in the observation group was lower than that in the control group ($p < 0.001$), with a statistically significant difference in the incidence of urethrocutaneous fistula ($p = 0.044$). No statistically significant differences were found in the incidences of urethral stricture, urethral diverticulum, or wound infection between the two groups ($p > 0.05$), as shown in **Table 3**.

Table 3. Comparison of postoperative complications between the two groups [n (%)]

Complication	Observation group (n = 52)	Control group (n = 44)	χ^2	*p*
Urethrocutaneous fistula	5(9.6)	11(25.0)	4.06	0.044
Urethral stricture	2(3.8)	6(13.6)	2.99	0.084
Urethral diverticulum	1(1.9)	4(9.1)	—	0.176
Wound infection	2(3.8)	3(6.8)	—	0.658
Total	11(21.2)	26(59.1)	14.48	< 0.001

Note: — indicates Fisher's exact test.

3.3. Stratified analysis and follow-up outcomes

After stratification by hypospadias type, the complication rates in the observation group were lower than those in the control group for both penile shaft type (5/31 vs. 13/26, $p = 0.006$) and proximal type (6/21 vs. 13/18, $p = 0.007$). Among 69 patients followed for at least 12 months who were able to cooperate (38 in the observation group, 31 in the control group), the observation group demonstrated superior maximum urinary flow rate [(13.1 ± 2.9) mL/s vs. (11.4 ± 3.0) mL/s, $p = 0.020$] and HOSE scores [(15.2 ± 1.4) vs. (13.8 ± 2.1), $p < 0.001$]. The reoperation rate during follow-up was 7.7% (4/52) in the observation group and 27.3% (12/44) in the control group, a statistically significant difference ($\chi^2 = 6.58$, $p = 0.010$).

4. Discussion

4.1. Anatomical basis and technical considerations

The inherent contradiction of the Duckett procedure lies in the fact that transecting the urethral plate resolves curvature but discards otherwise usable autologous urethra, thereby increasing the length of the tube required. The scattered corpus spongiosum surrounding the urethral plate possesses considerable blood supply, and the degree of abnormality worsens with hypospadias severity [7]. Multicenter data on proximal hypospadias indicate that technique selection depends on urethral plate width, glans size, and meatal location [10]. Distal

urethral mobilization represents a compromise between preservation and replacement. Three technical points should be emphasized: the dissection plane lies between the deep surface of the urethral plate and the tunica albuginea—too superficial risks injuring the submucosal vascular network, while too deep enters the corpus cavernosum; mobilization into the glans spongiosum is sufficient; and before anastomosis, the distal urethra should be grasped and advanced toward the glans to confirm absence of tension—if tension is evident, the approach should be converted to onlay or staged surgery.

4.2. Impact on postoperative complications

In this study, the neourethral length in the observation group was shortened by approximately 0.9 cm, the urethrocutaneous fistula rate decreased from 25.0% to 9.6%, and the overall complication rate decreased from 59.1% to 21.2%. Urethrocutaneous fistula arises from lack of corpus spongiosum support for the neourethra, poor local blood supply, and excessive tension at the anastomosis; shortening the tube simultaneously reduces the length of suture line and ischemic segment. Flap length itself is a risk factor for complications after the Duckett procedure [5]. In single-center follow-up, the postoperative fistula rate has been reported as high as 17.6% [6]; the control group in this study falls in the upper range of that interval, while the observation group was reduced to below 10%. Tang et al. found that one-stage Duckett had a lower fistula rate (7.56% vs. 18.49%) but a higher diverticulum rate (7.56% vs. 0.84%), suggesting that modified approaches each carry trade-offs; the trend toward lower diverticulum incidence in our observation group (1.9% vs. 9.1%) is consistent with their findings [11]. The difference in urethral stricture between the two groups did not reach statistical significance (3.8% vs. 13.6%, $p = 0.084$); insufficient sample size may account for the failure to detect a difference.

4.3. Indications and limitations

Distal urethral mobilization requires the presence of identifiable urethral plate or dysplastic urethral tissue distal to the meatus with reliable blood supply after mobilization. Three situations are unsuitable: residual curvature exceeding 30° requiring extensive release; prior surgery causing extensive local scarring and unclear tissue planes; and an extremely narrow or fibrotic, cord-like urethral plate. This study excluded cases requiring staged surgery, and the conclusions cannot be extrapolated to severe proximal hypospadias. The median follow-up in this series was less than 2 years; maximum urinary flow rate and HOSE scores reflect only midterm outcomes, and fistula and recurrent curvature may still occur during puberty [3]. This was a single-center retrospective cohort in which the technique was chosen by the surgeon based on intraoperative conditions, introducing selection bias, and the sample size was relatively small.

5. Conclusion

The Duckett procedure combined with distal urethral mobilization shortens the neourethral length without prolonging operative time, reduces the risk of urethrocutaneous fistula and reoperation, and improves midterm voiding function and objective scores. It is applicable to mid-penile and proximal hypospadias requiring transection of the urethral plate.

Funding

Baoding Science and Technology Program Project (Project No.: 2341ZF385)

Disclosure statement

The authors declare no conflict of interest.

References

[1] Springer A, van den Heijkant M, Baumann S, 2016, Worldwide Prevalence of Hypospadias. Journal of Pediatric Urology, 12(3): 152.e1–152.e7.

[2] van der Horst H, de Wall L, 2017, Hypospadias, All There Is to Know. European Journal of Pediatrics, 176(4): 435–441.

[3] Section of Urology, Society of Pediatric Surgery, Chinese Medical Association, 2018, Expert Consensus on Hypospadias. Chinese Journal of Pediatric Surgery, 39(12): 883–888.

[4] Fang Y, Song H, 2022, Surgical Advances in Severe Hypospadias. Chinese Journal of Pediatric Surgery, 43(9): 854–859.

[5] Fang Y, Song H, Sun N, et al., 2022, Risk Factors for Short-Term Complications After Transverse Preputial Island Flap Urethroplasty for Hypospadias. Journal of Clinical Pediatric Surgery, 21(1): 18–23.

[6] Li J, Liu P, Yang Z, et al., 2023, Reoperation Frequency After Transverse Preputial Island Flap Urethroplasty "Duckett's Technique" in Treatment of Severe Hypospadias: A Single Center Study. Frontiers in Pediatrics, 10: 1030649.

[7] Huang J, Huang Y, Shi X, et al., 2022, Phenotypic Modulation of Vascular Smooth Muscle Cells in the Corpus Spongiosum Surrounding the Urethral Plate in Hypospadias. Andrologia, 54(10): e14540.

[8] Edan O, 2021, Urethral Mobilization and Advancement Technique in Distal Types of Hypospadias: Short-Term Local Experience. Annals of Pediatric Surgery, 17(1): 60.

[9] Chen Y, Huang Y, Xie H, et al., 2022, Evaluation of Second-Stage Proximal Hypospadias Repair with Simultaneous Correction of Penoscrotal Transposition. Chinese Journal of Pediatric Surgery, 43(8): 704–708.

[10] Fang Y, Song H, Sun N, et al., 2022, Multicenter Study on Current Treatment Status and Short-Term Outcomes of Proximal Hypospadias. Chinese Journal of Pediatric Surgery, 43(8): 685–690.

[11] Tang H, Lyu C, Li Y, et al., 2022, Comparison of Complications and Influencing Factors Between One-Stage and Staged Duckett Procedures for Severe Hypospadias. Journal of Clinical Urology, 37(8): 626–630 + 634.

Bio-Byword Scientific Publishing remains neutral with regard to jurisdictional claims in published maps and institutional affiliations.

Integrated Services Platform of International Scientific Cooperation

Innoscience Research (Malaysia), which is global market oriented, was founded in 2016.Innoscience Research focuses on services based on scientific research. By cooperating with universities and scientific institutes all over the world, it performs medical researches to benefit human beings and promotes the interdisciplinary and international exchanges among researchers.

Innoscience Research covers biology, chemistry, physics and many other disciplines. It mainly focuses on the improvement of human health. It aims to promote the cooperation, exploration and exchange among researchers from different countries. By establishing platforms, Innoscience integrates the demands from different fields to realize the combination of clinical research and basic research and to accelerate and deepen the international scientific cooperation.

Cooperation Mode

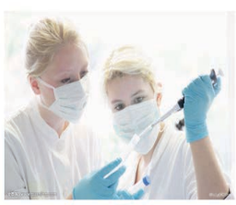


Clinical Workers



In-service Doctors





Foreign Researchers

China Collaborators



Oversea Collaborators



Hospital



University



Scientific institutions

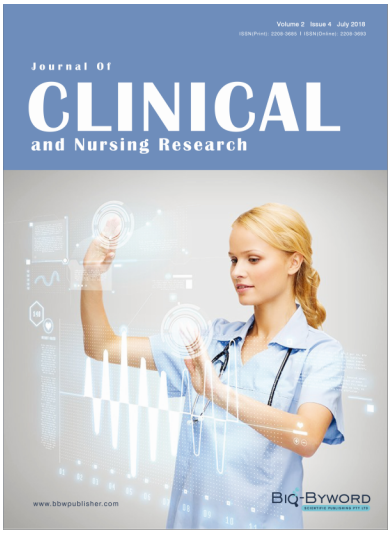
Our Journals



The *Journal of Architectural Research and Development* is an international peer-reviewed and open access journal which is devoted to establish a bridge between theory and practice in the fields of architectural and design research, urban planning and built environment research.

Topics covered but not limited to:

- Architectural design
- Architectural technology, including new technologies and energy saving technologies
- Architectural practice
- Urban planning
- Impacts of architecture on environment



Journal of Clinical and Nursing Research (JCNR) is an international, peer reviewed and open access journal that seeks to promote the development and exchange of knowledge which is directly relevant to all clinical and nursing research and practice. Articles which explore the meaning, prevention, treatment, outcome and impact of a high standard clinical and nursing practice and discipline are encouraged to be submitted as original article, review, case report, short communication and letters.

Topics covered by not limited to:

- Development of clinical and nursing research, evaluation, evidence-based practice and scientific enquiry
- Patients and family experiences of health care
- Clinical and nursing research to enhance patient safety and reduce harm to patients
- Ethics
- Clinical and Nursing history
- Medicine



Journal of Electronic Research and Application is an international, peer-reviewed and open access journal which publishes original articles, reviews, short communications, case studies and letters in the field of electronic research and application.

Topics covered but not limited to:

- Automation
- Circuit Analysis and Application
- Electric and Electronic Measurement Systems
- Electrical Engineering
- Electronic Materials
- Electronics and Communications Engineering
- Power Systems and Power Electronics
- Signal Processing
- Telecommunications Engineering
- Wireless and Mobile Communication